Journal of Wind Engineering & Industrial Aerodynamics 205 (2020) 104315

Contents lists available at ScienceDirect

Journal of Wind Engineering & Industrial Aerodynamics

journal homepage: www.elsevier.com/locate/jweia

CFD simulation of wind forces on ships in ports: Case study for the Rotterdam Cruise Terminal

A. Ricci [a,b,c,*], W.D. Janssen [d], H.J. van Wijhe [e], B. Blocken [a,b]

[a] Building Physics Section, Department of Civil Engineering, KU Leuven, Leuven, Belgium
[b] Unit Building Physics & Services, Department of the Built Environment, Eindhoven University of Technology, Eindhoven, the Netherlands
[c] Department of Civil, Chemical and Environmental Engineering (DICCA), Genoa, University of Genoa, Italy
[d] Port of Rotterdam, Rotterdam, the Netherlands
[e] Anchors & Connections, Amsterdam, the Netherlands

ARTICLE INFO

Keywords:
Nautical aerodynamics
Wind loads
Computational fluid dynamics (CFD)
Mooring forces port area

ABSTRACT

A nautical port is an aerodynamically complex built-up area. The wind forces on ships in ports can be very different from those at open sea. Knowledge of the wind conditions in ports and of the wind forces acting on ships in ports are essential for safe maneuvering and mooring. This paper presents a case study in which wind forces on a large cruise ship moored at the quay of the Rotterdam Cruise Terminal are determined by 3D steady RANS simulations. The simulated wind speeds and wind directions are validated by on-site measurements. A previous study in which simulated wind forces on a container ship were validated with wind-tunnel tests, is also mentioned here to justify the selection of computational parameters for the case study. Near to the Cruise Terminal quay various high-rise buildings exist that can influence the wind loads on the ship. It is shown that the presence of the high-rise buildings can yield locally amplified surface pressure, but that, due to the large size of the ship, the net horizontal force decreases. However, the net vertical upward force increases. For smaller ships, nearby high-rise buildings could yield an increase in both horizontal and vertical forces.

1. Introduction

Most nautical ports are situated in an aerodynamically complex environment with large spatial changes in aerodynamic roughness length and significant local temporal changes in geometry by the presence of large ships, moored and sailing in various positions. The wind forces on ships in ports can be very different from those on ships in open sea (Torre et al., 2019). Knowledge of these forces is important for safely maneuvering the ship in and out of the port and for safely mooring the ship (Repetto et al., 2018). The present policy in most ports worldwide is that ships are only admitted when, for a particular wind direction, the expected wind speed during the maneuvering operations will remain below a certain threshold wind speed. For example, for the largest port in Europe, the Port of Rotterdam, this threshold is typically around 11–13 m/s. However, this wind speed is generally measured at a fully exposed reference position. The presence of buildings in the port area however can increase or reduce the local wind speed and introduce large wind gradients, yielding higher or lower wind forces and moments than those that would occur in open sea, as also pointed out by Thoresen (2014). Therefore, more precise knowledge on the prediction of wind forces on ships in the port is required to fine-tune the admission policy of the port. Such knowledge is also required for the (tugboat) pilots as it provides them the necessary input for safely maneuvering the ship but also for their training in maneuvering simulators. Finally, the knowledge of wind forces on the ships in the port is necessary to ensure that safe working loads of bollards and fenders and buoys are not exceeded (e.g. Roubos et al., 2017, 2018). The importance of this knowledge is illustrated by the occurrence of incidents in ports where ships break loose while moored alongside or on buoys (Maritime Executive, 2017; DutchNews.nl, 2018, Reformatorisch Dagblad) or that control over the ship is lost during maneuvering (The Guardian, 2019; The Guardian News; Flows Magazine, 2019; Corriere della Sera 2020; Alexander Farstad; La Sicilia 2019; La Sicilia), which can cause substantial damage to the ship and the port infrastructure.

The above-mentioned difficulties and concerns are amplified by the continuing increase in ship size over the past decades. This increase has been observed both for container ships (Gomez Paz et al., 2015; Merk, 2015; Martin et al., 2015; van Hassel et al., 2016; Malchow, 2017; Lu and

* Corresponding author. Building Physics Section, Department of Civil Engineering, KU Leuven, Leuven, Belgium.
E-mail address: a.ricci@tue.nl (A. Ricci).

https://doi.org/10.1016/j.jweia.2020.104315
Received 27 April 2020; Received in revised form 17 July 2020; Accepted 17 July 2020
Available online 21 August 2020

Yeh, 2019) and cruise ships (Sun et al., 2014; Bucci et al., 2016; Castillo-Manzano and Lopez-Valpuesta, 2018). For example, the cruise ship *Oasis of the Seas*, which had its maiden voyage in 2009, has an overall length of 360 m and a maximum beam (i.e. width) of 60.5 m and a waterline beam of 47 m (DNVVessel Register, 2019). Fig. 1 compares the size of the *Oasis of the Seas* with that of *Titanic*, which was a state-of-the-art cruise ship at the beginning of the previous century. Cruise ships and container ships are similar in that they are both characterized by large overall sizes but also by the fact that the majority of the ship's lateral surfaces are situated above the waterline, yielding a large windage area, which increases the contribution of the wind loads to the total loads on the ship. As an example, the *Oasis of the Seas* has a height of 65 m above the water line and a depth of 22.55 m (DNVVessel Register, 2019). A complicating factor for container ships is that the positions of containers stowed above deck can vary, which induces changes in the wind flow field.

Wind forces on ships at *open sea* conditions are generally determined by either wind-tunnel (WT) tests on reduced-scale models or by computational fluid dynamics (CFD) simulations, or by simplified methods based on databases of WT test results. However, as recently stressed by Torre et al. (2019), measured wind forces on ships in open areas may be very different than those measured on ships moored in *port areas* since the latter can highly depend on the surrounding buildings, cranes and other obstacles. Indeed, as largely confirmed by recent publications dealing with wind flow modeling in complex port areas by experimental (as on-site measurements and WT testing) and numerical analyses (e.g. Solari et al., 2012; Burlando et al., 2014; Repetto et al., 2017, 2018; Ricci et al., 2017a,b, 2018, 2019, 2020; Blocken et al., 2015), local and large-scale forcing effects can strongly affect the atmospheric boundary layer (ABL) development especially in its lower part, the so-called urban boundary layer (UBL). To determine the wind forces in such cases, dedicated WT tests or CFD simulations including a large part of the port area should be performed. Attention to the interaction of the position of a ship and its environment should also be taken into account.

In the last decades, a wide range of WT tests were carried out on different types of ships in open sea-like conditions to investigate the air resistance and airwake produced by superstructures (e.g. Hughes, 1930, 1932; Mutimer, 1955; Gould, 1967; Benham, 1977; Andersson, 1978; Bardera Mora, 2014) and to determine wind forces and wind load coefficients (e.g. Shearer et al., 1961; Aage, 1968; van Berlekom, 1981; Owens and Palo, 1982; OCIMF, 1994; Blendermann, 1995, 1997; Haddara and Guedes Soares, 1999; Ocimf, Sigtto, 1985; Fujiwara et al., 2009; Andersen, 2013; Torre et al., 2019). Isherwood (1972), Hong (1991), Blendermann (1994) and Fujiwara and Nimura (2005) presented a mathematical model to estimate wind forces on ships based on a regression analysis of a wide range of WT data. Valčič et al. (2020) applied pattern recognition to estimate wind loads on ships and marine objects. Several CFD studies were published, few of which included a comparison between CFD simulations and WT tests. Koop et al. (2012) compared WT tests and CFD simulations for five different ship types: (1) a Moss type LNG carrier; (2) a membrane type LNG carrier; (3) a shuttle tanker at 10 m draft; (4) a shuttle tanker at 22 m draft; and (5) an FPSO. Wnęk and Guedes Soares (2015) focused on the wind load on an LNG carrier with a specific geometrical shape. Both Koop et al. (2012) and Wnęk and Guedes Soares (2015) obtained good results when comparing the force coefficients C_X, C_Y and C_N obtained from CFD simulations with WT data. However, the results of the comparison were provided in graphical form and not in an overall percentage difference. None of these studies however provided a detailed analysis of the impact of geometrical simplifications on the predicted wind loads. To address this issue, Janssen et al. (2017) computed the wind load coefficients on a post-Panamax 9000 + TEU container ship with the 3D steady Reynolds-averaged Navier-Stokes (RANS) approach with the realizable k-ε model for closure using four different geometrical representations of the same ship. Comparison of numerical and experimental results in terms of total wind load on the ship by Andersen (2013) showed a 37.9% average deviation for the most simplified geometry but only a 5.9% average deviation for the most detailed geometry. Wang et al. (2019) analyzed the wind load coefficients for the superstructure of a 1900TEU container ship with CFD simulations and WT tests. The CFD simulations were performed with the unsteady RANS approach and the *SST* k-ω model for closure, demonstrating a good agreement for both longitudinal and transverse wind load coefficients. Some other CFD studies dealing with similar topics, but not validated through experimental data, were also published (e.g. Brizzolara and Rizzuto, 2006; Saydam and Taylan, 2018).

While most studies focused on wind loads on a ship in open sea-like conditions, some others have considered more complicated conditions. Crudu et al. (2016) analyzed the wind forces on two ships with varying speed and wind direction, representing movement over a river. Paulauskas et al. (2009) assessed the theoretical approach to determine the wind loads on mooring ships and the efficiency of possible windscreens to reduce the wind loads in open port areas. Van Zwijnsvoorde and Vantorre (2017) determined the motions and the forces on a moored 18000 TEU container vessel due to ship passages, using the potential software ROPES and an in-house developed software tool. Torre et al. (2019) carried out WT tests on a reduced-scale model 1:600 of a container ship. The longitudinal and transverse forces and yaw moment were measured for three configurations: (1) isolated ship, (2) ship and quay, (3) ship, quay and another shielding ship upwind. However, to the best of our knowledge, Aage et al. (1997) carried out WT tests on a ferry model in a port including the effects of surrounding buildings and CFD simulations only on a ferry model (without surrounding). In particular, because cruise ships tend to moor very close to the built environment, the question arises as to whether the presence of high-rise buildings can increase the wind loads and moments on the ship. Such a study requires the employment of high-resolution CFD simulations validated with experimental data.

This is also the main goal of the present paper in which wind forces on a cruise ship (the *Oasis of the Seas*) moored at the quay of the Rotterdam

Fig. 1. *Oasis of the Seas* (2009) compared to the *Titanic* (1909). Sources: *dumpert.nl* (Telegraaf Media Groep).

Cruise Terminal are determined by 3D steady RANS simulations. This Cruise Terminal is situated more than 20 km inland, surrounded by a moderately dense built-up area and characterized by the presence of several high-rise buildings on the quay. The RANS approach is adopted as it is most commonly used in computational wind engineering research and practice (Stathopoulos, 2002; Hanjalic, 2005; Baker, 2007; Franke et al., 2007; Blocken, 2014, 2018; Hang et al., 2018). The CFD simulations are accompanied by a validation study based on on-site wind speed measurements. The wind forces exerted on the *Oasis of the Seas* are evaluated based on the RANS simulations. A previous study by Janssen et al. (2017), in which wind forces on a container ship in open sea-like conditions were determined by 3D steady RANS simulations and validated by WT tests (by Andersen, 2013), is reported here to justify the use of the steady RANS approach for evaluation the forces. This previous study also guided the level of geometrical simplification to be adopted for the cruise ship *Oasis of the Seas* moored at the quay of the Cruise Terminal of the Port of Rotterdam, and it indicated the computational settings and parameters required to obtain accurate simulation results.

This study was part of a series of projects performed by Eindhoven University of Technology and its partners for the Port of Rotterdam, including measurements and CFD simulations of wind conditions in the Maasvlakte 1 and 2 and the CFD simulations for the Cruise Terminal, reported in this paper. In the present study, the specific request of the Port Authority was to study to the wind loads on the *Oasis of the Seas* for its first visit to the Port of Rotterdam in September 2014 and to allow the determination of the resulting forces on bollards and fenders.

Although the investigation in the present paper mainly focuses on a ship moored at the quay of the port of a European city, the same methodology could also be applied to different scenarios worldwide. For instance, ships approaching the entry of a port, ships crossing sea locks inside a port area, or simply ships navigating through a narrow canal inside historical cities can experience strong local wind conditions which may lead to unsafe conditions.

The paper is structured as follows. In Section 2, the case study area and its surroundings are described. Section 3 presents the first validation study, while Section 4 presents the second one. Section 5 provides the CFD results of the wind forces on the ship for different wind directions and analyzes the effect of the buildings on the wind forces. Finally, Section 6 concludes the paper.

2. Studied area and surroundings

The Port of Rotterdam is the largest port in Europe. It covers 127.13 km^2 and stretches over a total distance of 42 km (Fig. 2a) (Port of Rotterdam, 2020). The Rotterdam Cruise Terminal is situated approximately 30 km inland (Fig. 2b). In the past, the Cruise Terminal served as arrival and departure location of the Holland America Line. Today, it is considered industrial heritage, it was renewed and it is still used by large passenger ships that visit Rotterdam. It is located at the so-called *"Kop van Zuid"* area close to Rotterdam city center (Fig. 2c). The Kop van Zuid

Fig. 2. (*a*) Map of Port of Rotterdam with indication of area around Cruise Terminal (source: *Google Earth*); (*b*) Detail view with indication of Cruise Terminal (source: *Google Earth*); (*c*) Photo from south (source: *Google Earth*); (*d*) Photo from west (source: *NOS.nl*).

is a newly developed area also known as *"Manhattan on the Maas"*, indicative of the high-rise buildings present at this location. In September 2014, one of the largest passenger ships in the world, the *Oasis of the Seas*, made her first visit to the renewed Cruise Terminal in Rotterdam (Fig. 2d). This prospect marked the start of the study reported in this paper. Fig. 3a indicates the wider surroundings of the cruise terminal with indication of the aerodynamic roughness length z_0 of upstream areas covering a 5 km distance. The values of z_0 were determined based on the updated Davenport roughness classification (Wieringa, 1992). Fig. 3b indicates the local surface height approximately above the mean water level for Amsterdam in absence of water motion (or Normaal Amsterdams Peil, NAP), with the light gray color indicating NAP (Ministry of Defence, 2020).

3. CFD validation study I: wind forces on a ship in open sea-like conditions

This study is mentioned here to justify the level of geometrical simplification adopted for the cruise ship simulated in the Cruise Terminal of the Port of Rotterdam and to indicate the computational settings and parameters required to accurate simulation results (Section 4). It was

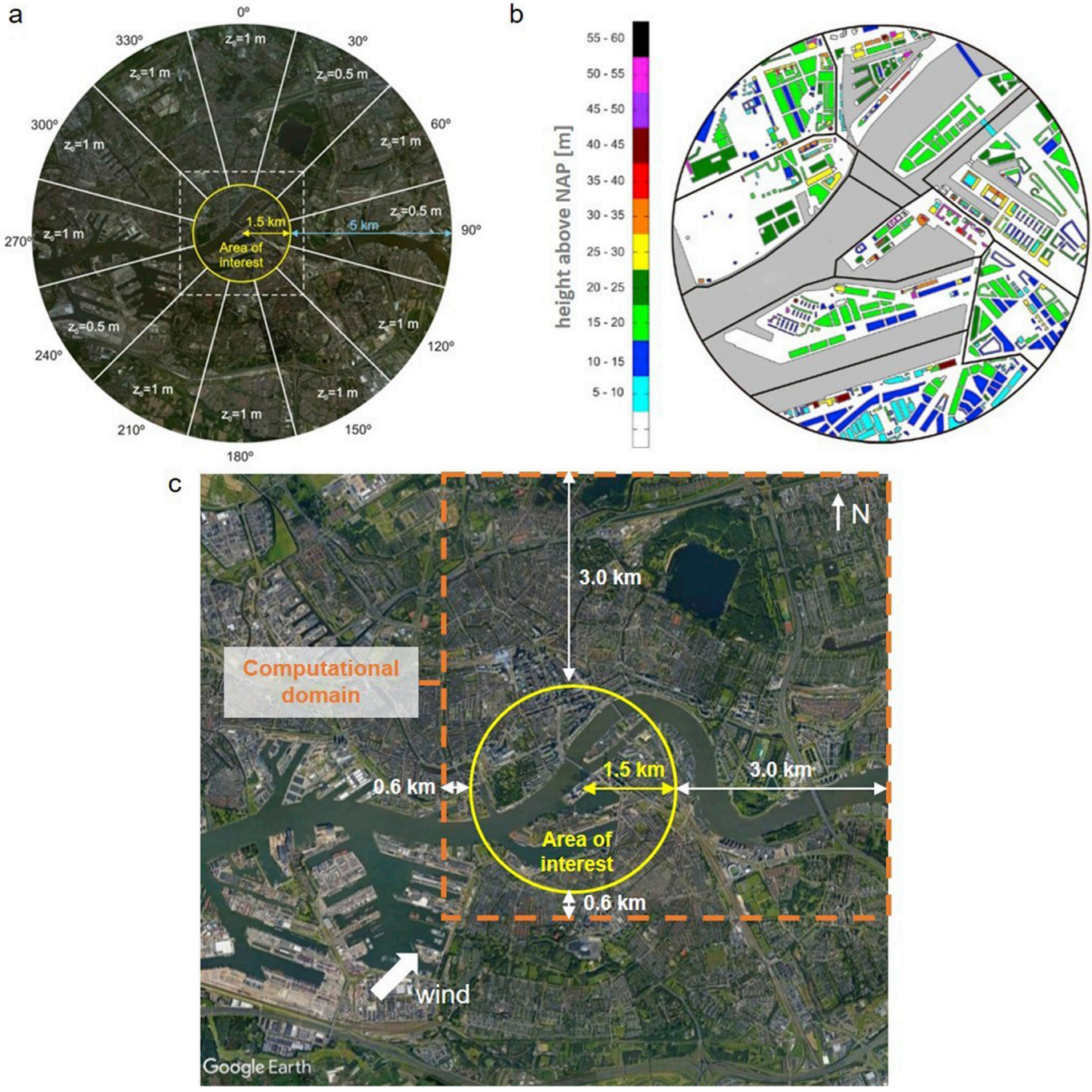

Fig. 3. (*a*) Aerodynamic roughness length for terrain surrounding the area of interest. (*b*) Height above NAP for immediate surroundings of the Cruise Terminal. (*c*) Example of a computational domain for the South-West reference wind directions (θ).

published in full previously (Janssen et al., 2017). Note that cruise ships and container ships are similar in that they both have similar sizes and large windage areas. Therefore, it is only briefly reported here.

3.1. Wind-tunnel tests

Andersen (2013) reported WT tests to determine the wind force coefficients on a post-Panamax container ship. A reduced-scale model (1:450) was tested in the closed low-speed boundary layer wind tunnel of FORCE Technology with dimensions W x H x $L = 1 \times 0.7 \times 2.6$ m^3 and chamfered corners of 0.11 m. The container ship was placed in the middle of a turntable with the center point located at 0.79 m from the inlet of the measurement section. The fully loaded ship size, with containers stacked 7 high, was about W x H x $L = 0.101 \times 0.077 \times 0.75$ m^3 (Fig. 4a). In full scale this container ship is approximately 45 m wide, 35 m high and 340 m long. The WT tests were performed for 19 different reference wind directions at 10° intervals. Since the ship is symmetrical over its length x-axis, measurements for the other 17 reference wind directions are not performed. The results of the tests will be reported together with the CFD simulation results in Section 3.3.

3.2. CFD simulations: computational settings and parameters

Janssen et al. (2017) analyzed the wind load coefficients for different configurations of the ship resulting from various degrees of geometrical simplifications, from a simplified rectangular prism to the actual geometry (Fig. 4a–g). The geometries C and D took into account the spacing between the container stacks and geometry D also took into account the detailed geometry of the bow and stern of the ship. The computational domain was taken equal to the geometry of the WT test section (i.e. at scale 1:450), however without the chamfered corners (Fig. 4b). For several ship orientations in the WT, the blockage ratio was too high (equal to 7.4%). Both WT and CFD results were corrected for blockage following the guidelines of the Engineering Sciences Data Unit ESDU 80024, 1980. However, these ESDU guidelines were not developed for ship geometries. As a result, matching the WT test section and the computational domain and applying the same blockage corrections to WT and CFD results was important in order not to compromise the WT vs. CFD comparison.

High-resolution computational grids were created for each configuration. The computational grid of different configurations were built by Gambit 2.4.6 using the grid-generation technique proposed by van Hooff and Blocken (2010) and the best practice guidelines for CFD (Franke et al., 2007; Tominaga et al., 2008). All configurations (A, B, C, D) fit into a rectangular box with dimensions L x W x $H = 0.740 \times 0.101 \times 0.077$ m^3 ($333.00 \times 45.45 \times 34.65$ m^3 in full scale). A growth rate equal to 1.1–1.3 was used between the ship and the outer domain. A maximum grid size of about 0.03 m was used at the outlet face. Configuration A was the simplest, representing the above-mentioned rectangular box (Fig. 4d). The box was discretized by 206, 24, 32 cells over the length, width and height, respectively. The cell resolution footprint on the hull was about 0.0036×0.0022 m^2 (i.e. 1.6×1.0 m^2 at full scale). The final grid counted about 2.87 million cells. For configurations B, C and D, the level of geometrical detail was gradually increased in order to properly model the containers stacked 7 high, the bow and the hull of the ship (Fig. 4e,f, g). For configuration B, the space between the container stacks was neglected and both the hull and bow were simplified. A cell resolution footprint on the hull equal to 0.0044×0.0044 m^2 (i.e. 2×2 m^2 at full scale) was adopted. The final grid counted about 1.54 million cells (Fig. 4e). For configuration C, the space in-between the container stakes was modeled as well as the bow, but the hull geometry was kept simplified. The cell resolution footprint on the hull was taken equal to 0.0022×0.0022 m^2 (i.e. 1×1 m^2 at full scale). The final grid counted about 3.97 million cells (Fig. 4f). For configuration D, a more detailed

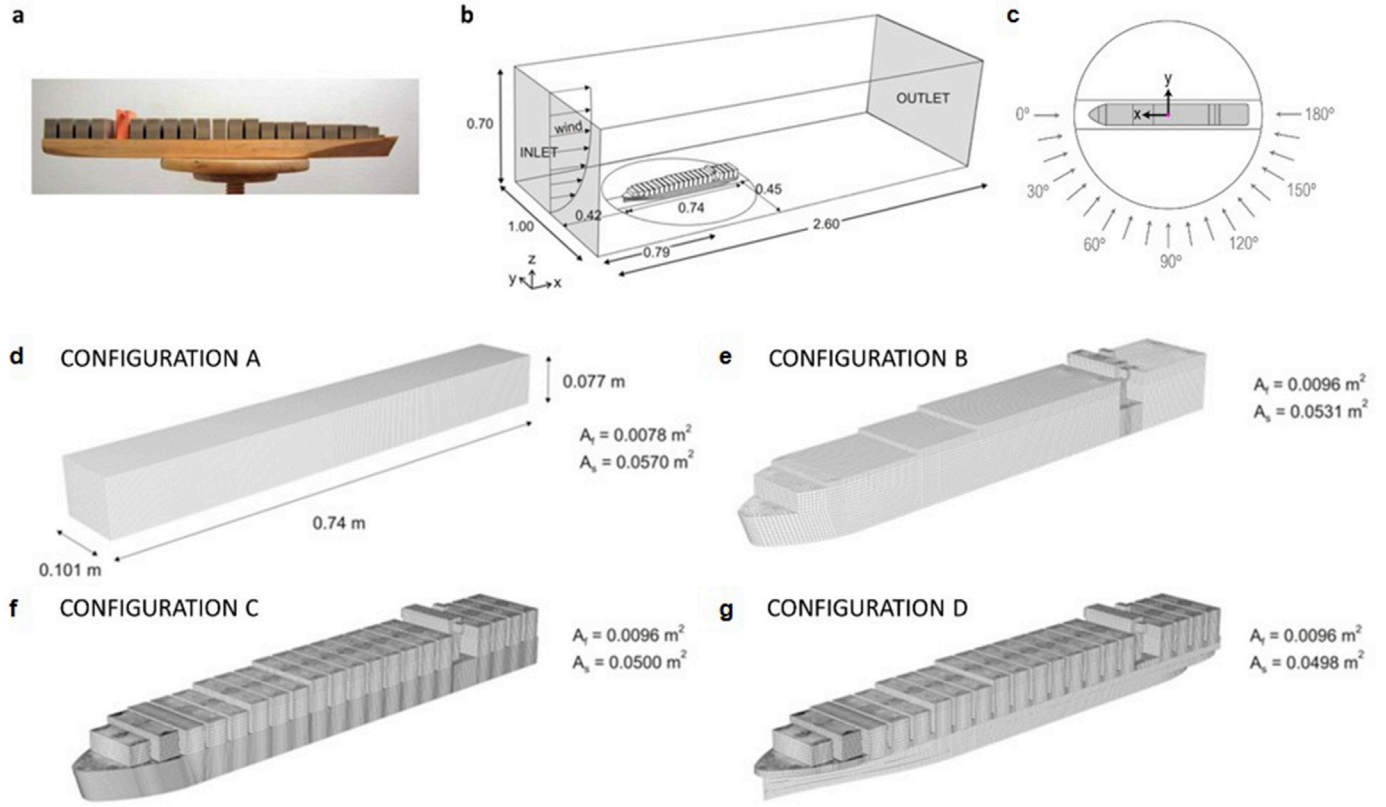

Fig. 4. (*a*) Wind-tunnel model by Andersen (2013). (*b*) Computational domain by Janssen et al. (2017). (*c*) Definition of reference wind directions (α) and Cartesian coordinates. (*d-g*) Computational grids by Janssen et al. (2017) for four ship geometries with increasing geometrical detail (Config. A: 2,866,376 cells; Config. B: 1,541, 840 cells; Config. C: 3,970,994 cells and Config. D: 3,905,906 cells).

bow and hull geometry were considered based on the drawings of Andersen (2013). A cell resolution footprint on the hull equal to 0.0022 × 0.0022 m^2, (i.e. 1 × 1 m^2 in full scale) was adopted. The final grid counted about 3.90 million cells (Fig. 4g). Further details on these grids can be found in Janssen et al. (2017).

The inlet boundary conditions were based on the WT measurements. The roughness of the bottom of the domain was implemented by means of the parameters k_S (i.e. equivalent sand-grain roughness height) and C_S (i.e. roughness constant) in the standard wall functions. The k_S was calculated in accordance to Blocken et al. (2007a, 2007b) as follows:

$$k_S = \frac{9.793\, z_0}{C_S} \tag{1}$$

For the aerodynamic roughness length (z_0) a full-scale value of 0.0002 m, corresponding to a reduced-scale value of 4.44 × 10^{-7} m, was considered from the updated Davenport roughness classification (Wieringa, 1992). The value of C_S was chosen equal to 1 to adhere with the condition $y_P > k_S$ (where y_P is the distance between the center point of the wall-adjacent cell and the wall). At the outlet, zero static gauge pressure was imposed. The 3D steady RANS equations were solved with

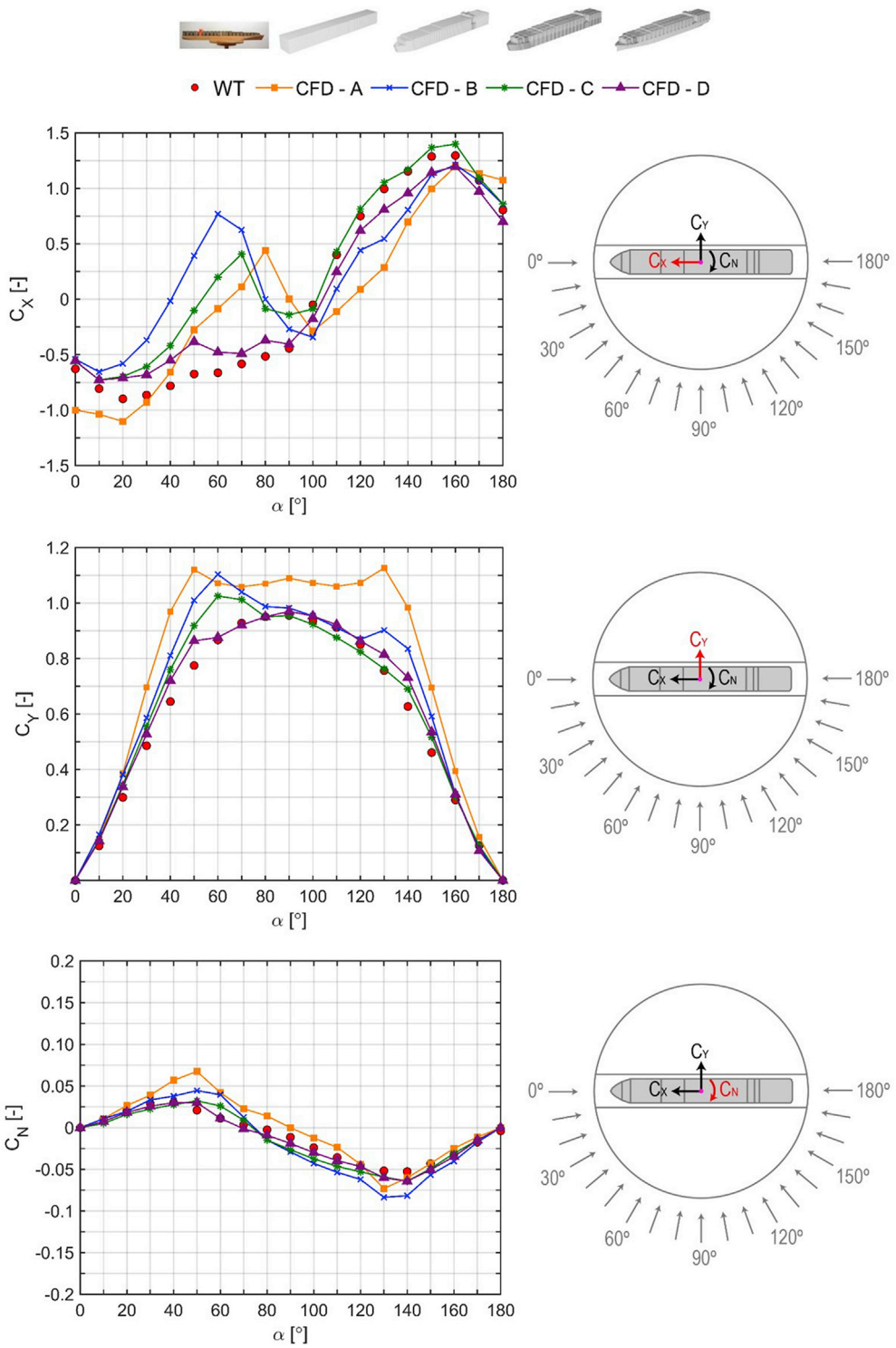

Fig. 5. Comparison of force and moment coefficients (C_X, C_Y, C_N) by WT tests and CFD simulations as a function of reference wind direction (α) on the ship.

the commercial CFD code Ansys Fluent 15 using the control volume method (ANSYS Fluent, 2013). The realizable k-ε turbulence model was used to provide closure (Shih et al., 1995). Second-order upwind discretization schemes were used for both the convective and viscous terms of the governing equations (Ferziger and Perić, 2002; Versteeg and Malalasekera, 2007). The SIMPLE algorithm was used for pressure-velocity coupling and standard pressure interpolation was used. Convergence was assumed to be obtained when all the scaled residuals had leveled off.

3.3. CFD validation

A comparison between the WT model by Andersen (2013) and the computational domain of different geometrical configurations (A, B, C and D) by Janssen et al. (2017) is shown in Fig. 4. The Cartesian coordinate system and the definition of the reference wind directions are shown in Fig. 4c. The longitudinal force, X, the lateral force, Y, and the moment around the z-axis, N, are made non-dimensional in Eqs. (2)–(4) as follows:

$$C_X = \frac{X}{\frac{1}{2}\rho U^2 A_f} \tag{2}$$

$$C_Y = \frac{Y}{\frac{1}{2}\rho U^2 A_s} \tag{3}$$

$$C_N = \frac{N}{\frac{1}{2}\rho U^2 A_s L_{oa}} \tag{4}$$

where ρ is the air density (equal to 1.225 kg/m^3 at 15 °C), U the approach-flow wind velocity (m/s), A_f the projected front area of the ship (m^2), A_s the projected side area of the ship (m^2) and L_{oa} the length overall of the ship. Note that C_N is positive when the ship bow moves to starboard.

Fig. 5 compares the computed force and moment coefficients for the four ship geometries (i.e. configurations A, B, C and D - see also Fig. 4d,e,f,g) with the results from the WT tests. The figure clearly shows the improving agreement with the WT data for more detailed CFD model geometries and generally higher wind loads by CFD compared to WT. The average of the absolute differences (summed over all reference wind directions, α) between the measurements and the CFD results for configurations A, B, C and D are 37.9%, 17.1%, 6.9% and 5.9%, respectively.

In conclusion, the combination of the current grid resolution (i.e. cell footprint on the hull approximately 0.0022 × 0.0022 m^2 at reduced scale for configuration D), turbulence model (i.e. realizable k-ε) and near-wall treatment by standard wall functions provides a satisfactory agreement with the WT data when one of the most detailed geometries is considered.

4. CFD validation study II: wind velocities near cruise terminal

4.1. On-site measurements

A measurement campaign from December 2013 to July 2014 was performed with a dual purpose: (*i*) to provide experimental data for CFD validation; (*ii*) to provide real-time input data of reference wind conditions for the actual assessment of wind conditions during the days of mooring of cruise ships.

3D ultrasonic anemometers were installed at four positions on the quay on top of lamp posts at 10 m above the ground (Fig. 6a,c). Additionally, a fifth 3D ultrasonic anemometer was placed on top of the roof of the World Port Center (WPC) building (Fig. 6b). This last position is termed reference position in the remainder of this paper and the measured mean wind speed at this location is denoted U_{ref}. The fifth anemometer was placed on a mast at 8 m above the roof of the WPC to ensure that it was located outside the rooftop recirculation area for all reference wind directions. Because this measurement position was on top of one of the highest buildings in the area, it would only be influenced by other high-rise buildings for a few specific reference wind directions, particularly 60° and 150° due to the presence of a few other high-rise buildings in these wind direction sectors (see Fig. 6a,c). The total measurement height was about 133 m above NAP.

The measurements were performed at a sampling rate of 1 Hz and averaged into 10-min data of wind velocity and wind direction. The 10-min averaged data at positions 1 to 4 were converted into wind speed ratios ($\gamma = U/U_{ref}$). These ratios were clustered into 12 wind direction sectors around the median values 0°, 30°, 60°, …, 330°. Before averaging the 10-min wind speed ratios in each wind direction sector, the following data were manually removed: (1) events with U_{ref} lower than 5 m/s (Pasquill, 1961) to exclude thermal effects and only focus on high wind speed conditions, which are those relevant for the present study; (2) data with U_{ref} from the wind direction sectors 60° and 150°, for which the reference measurement position was in the wake of nearby high-rise buildings; (3) data sampled while ships were berthed at the quay because these ships evidently influenced the measurements and because the validation study would be performed without berthed ships; (4) data with wind speed measurements showing strong wind direction fluctuations indicative of their position in a von Kármán vortex street behind nearby buildings. Therefore, 10-min data with a standard deviation of the wind direction of 35° and more were excluded from the data. After

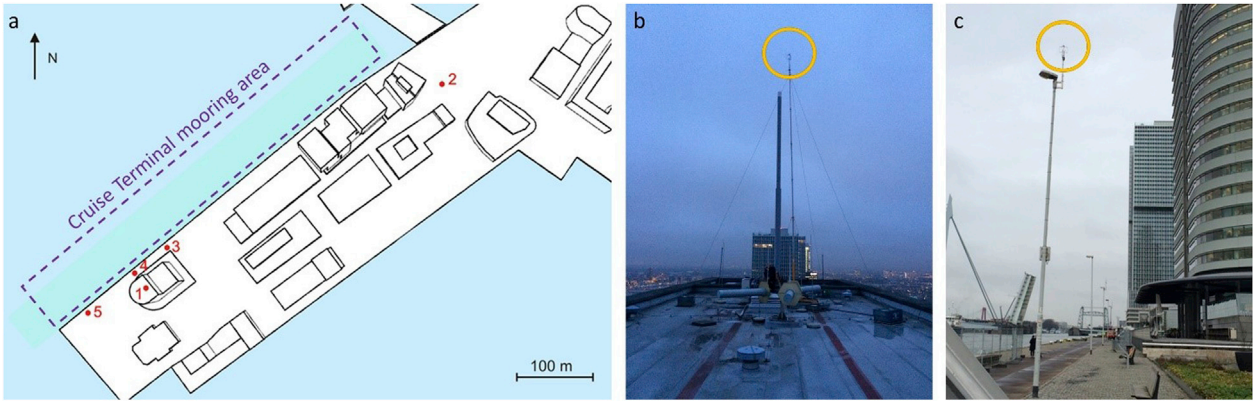

Fig. 6. (*a*) Location of measurement positions 1–5. (*b,c*) Photos of measurement positions 1 and 5.

excluding these data, the 10-min wind speed ratios in every wind direction sector were averaged resulting in a single value per wind direction sector.

4.2. CFD simulations: computational settings and parameters

For the validation study, the Cruise Terminal without berthed ships was considered. The computational domain had dimensions L x W x H =

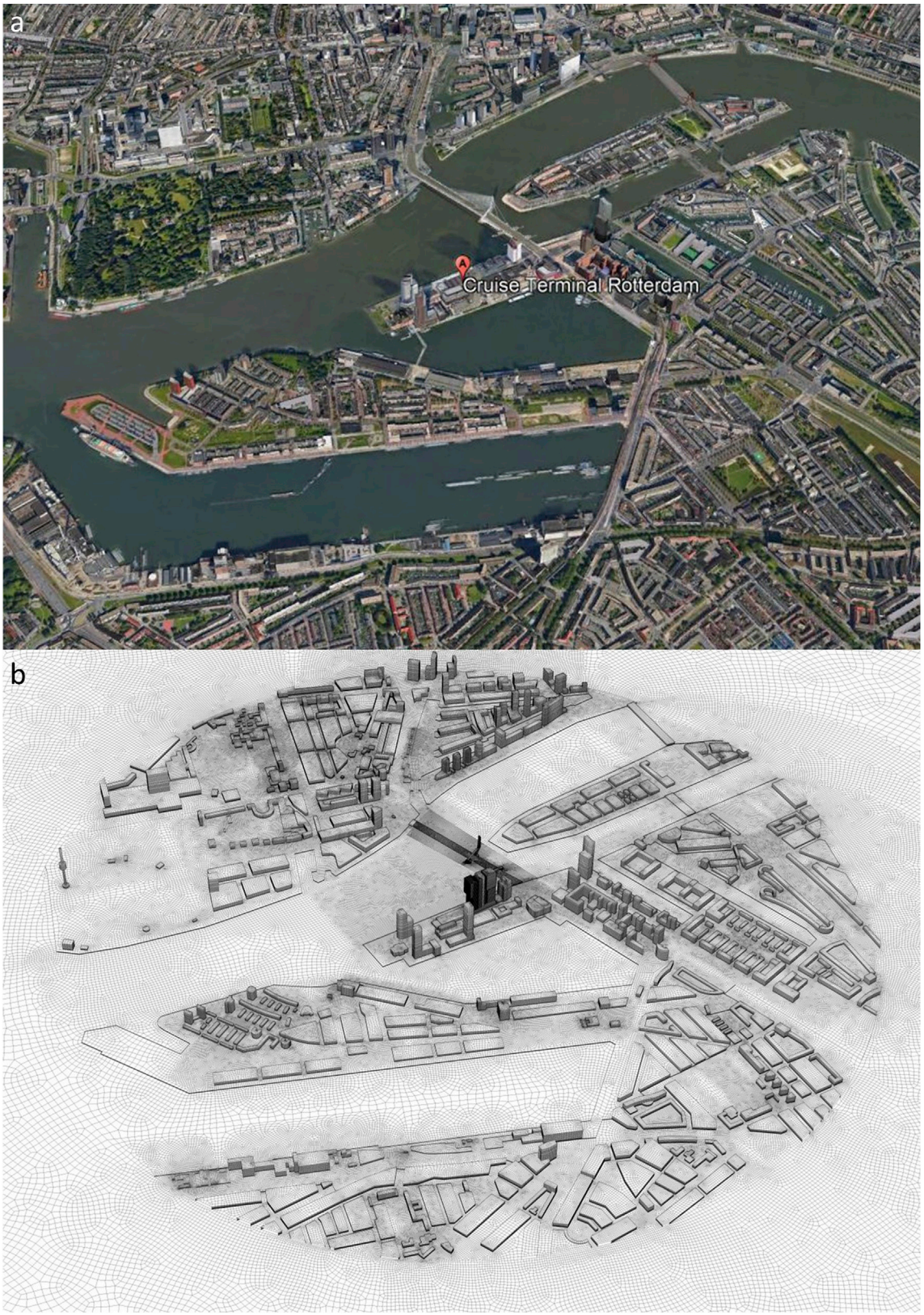

Fig. 7. Cruise Terminal and surrounding area: (*a*) photo (source: *Google Earth*) and (*b*) computational grid. Total cell count: 55 million.

$6.6 \times 6.6 \times 1.0\ km^3$. It is indicated by the dashed rectangle in Fig. 3c. The bottom of the domain consisted of a circular area of interest with a radius of 1500 m that contained the explicitly modeled buildings (i.e. those modeled with their actual shape and size), and a square domain around it in which buildings were modeled implicitly (i.e. by providing appropriate values of the equivalent sand-grain roughness height and roughness constant in the wall functions) (Figs. 3c and 7a). A high-resolution computational grid (Fig. 7b) was created using the surface extrusion grid technique presented by van Hooff and Blocken (2010) and following the best practice guidelines by Franke et al. (2007), Tominaga et al. (2008) and Blocken (2015). The resulting grid contains approximately 55 million cells, which are mostly hexahedral cells (Fig. 7b). At the inlet of the domain a logarithmic mean wind speed profile (Eq. (5)), representing a neutral ABL, is imposed with aerodynamic roughness length z_0 as specified in Fig. 3a. Two different z_0 were used each for a different wind direction: $z_0 = 0.5$ m for the wind directions 30°, 90° and 240°, and $z_0 =$ 1 m for the other wind directions. A reference wind speed (U_{ref}) equal to 5 m/s at the reference height (z_{ref}) of 10 m above NAP was assumed to calculate the inlet wind speed profile. Turbulent kinetic energy (k) and turbulence dissipation rate (ε) profiles are calculated as follows (Eqs. (6) and (7)) (Richards and Hoxey, 1993):

$$U = \frac{u^*}{\kappa}\ln\left(\frac{z+z_0}{z_0}\right) \tag{5}$$

$$k = \frac{(u^*)^2}{\sqrt{C_\mu}} \tag{6}$$

$$\varepsilon = \frac{(u^*)^3}{\kappa(z+z_0)} \tag{7}$$

In Eqs. (5)–(7), u^* the friction velocity, κ is the von Kármán constant (equal to 0.42) and C_μ is a constant (equal to 0.09). At the outlet, zero static gauge pressure is imposed. The top of the domain is modeled as a slip wall. The roughness of the bottom of the computational domain is taken into account by standard wall functions (Launder and Spalding, 1974) with the sand-grain roughness modification by Cebeci and Bradshaw (1977). The aerodynamic length (z_0) value is converted into the corresponding equivalent sand-grain roughness height (k_S) by Eq. (1).

Water areas are given an aerodynamic roughness length z_0 of 0.0002 m while the solid ground surface in the explicitly modeled area between the buildings has a z_0 of 0.03 m as determined by on-site measurements in an urban area by (Blocken and Persoon, 2009) (Table 1). For land areas outside the circular area of interest z_0 is either 0.5 m or 0.63 m taking the maximum values for the roughness parameters: $k_S = 0.875$ m (which is limited to half the first cell height above land) and $C_S = 7$ and the circular area of interest is given a z_0, while in the area of interest the buildings are modeled explicitly.

The 3D steady RANS equations are solved with the commercial CFD code Ansys Fluent 15. The realizable k-ε turbulence model (Shih et al., 1995) is used for closure. Second-order upwind discretization schemes are used for both the convective and viscous terms of the governing equations (Ferziger and Perić, 2002; Versteeg and Malalasekera, 2007).

Table 1
Aerodynamic roughness length (z_0), equivalent sand-grain roughness height (k_S) and roughness constant (C_S) values for the horizontal surfaces in the computational domain.

roughness patch	z_0 [m]	k_S [m]	C_S [-]
water surfaces	0.0002	0.002	1
ground surface inside explicitly modeled area	0.03	0.29	1
park (near Euromast)	0.29	0.4	7
surrounding area: urban	1	0.875	7
surrounding area: urban and water surfaces	0.5	0.7	7

The SIMPLEC algorithm is used for pressure-velocity coupling and second-order pressure interpolation is used. The simulations were terminated when the scaled version of total sum of residuals over 55 million cells did not show any further reduction with increasing number of iterations. The following minimum values were reached: z-velocity: 10^{-8}, k, x- and y-velocity: 10^{-7}, ε: 10^{-6} and continuity: 10^{-5}.

4.3. CFD validation

Figs. 8 and 9 compare the measured and computed, for 12 reference wind directions (θ), wind speed ratios U/U_{ref} including also the data where (*i*) the reference measurement position was in the wake of nearby high-rise buildings (i.e. $\theta = 60°$ and $\theta = 150°$) and the data where (*ii*) one or more of the positions 2 to 5 were situated in the vortex street behind nearby buildings. These data clearly show the largest deviation between the CFD simulations and the measurements. Fig. 10 summarizes the results for all reference wind directions however excluding the specific data mentioned in items (*i*) and (*ii*). Overall, a fair agreement is observed, with deviations between CFD and measurements generally below 30%. The results of the present work are in line with previous similar studies (e.g. Janssen et al., 2013; Blocken et al., 2015; Ricci et al., 2019) carried out by on-site measurements, WT tests and CFD simulations on port areas surrounded by complex urban environments, where deviations between measured and computed data where below 30%. This 30% deviation is likely the combination of an ensemble of deviations caused by the geometrical simplifications introduced to buildings and other obstacles (Carpentieri and Robins, 2015; Ricci et al., 2017a), the surface roughness applied to the ground (Ricci et al., 2020), the adopted steady RANS approach and the selected turbulence model. In particular, the inability of the steady RANS approach to accurately predict separation and recirculation and von Karman vortex shedding in the wake is considered as a major contributor to the deviations. Instead of 3D steady RANS approach one could consider Large Eddy Simulation (LES) or a hybrid RANS/LES approaches, however at a much higher computational cost. In addition, while for RANS simulations extensive best practice guidelines have been proposed in the past decades to guide CFD users towards accurate and reliable CFD simulations (Casey and Wintergerste, 2000; Britter and Schatzmann, 2007; Franke et al., 2007; Tominaga et al., 2008; Blocken, 2015), such guidelines are not yet available for LES simulations (Blocken, 2018).

Based on the validation studies in Sections 3 and 4, the next section will focus on CFD simulations for the Cruise Terminal with the cruise ship *Oasis of the Seas* present along the quay.

5. CFD simulations with cruise ship moored at the quay

5.1. CFD simulations: computational settings and parameters

For this part of the case study, the *Oasis of the Seas* is moored at the quay of the Cruise Terminal as shown in Fig. 11. The computational domain and the computational grid are the same as in Section 4 apart from the addition of the cruise ship. The computational grid on and around the cruise ship is based on the grid used in Section 3, however, with a somewhat higher grid resolution in order to include some more details of the cruise ship superstructure. The surface of the ship is discretized with cells of about $1 \times 1\ m^2$. The total number of cells is about 58 million, which are mostly hexahedral cells. The boundary conditions and solver settings are identical to those in Section 4.

5.2. CFD results: velocity fields

Figs. 12 and 13 present CFD results of the wind velocity field at a height of 5 m above NAP, for 12 reference wind directions (θ). Note that in Fig. 12c and f, the colorbar range is 0–2 rather than 0 to 1.2 as in the other figures. This is due to the above-mentioned problem of the reference position being situated in the wake of nearby high-rise buildings,

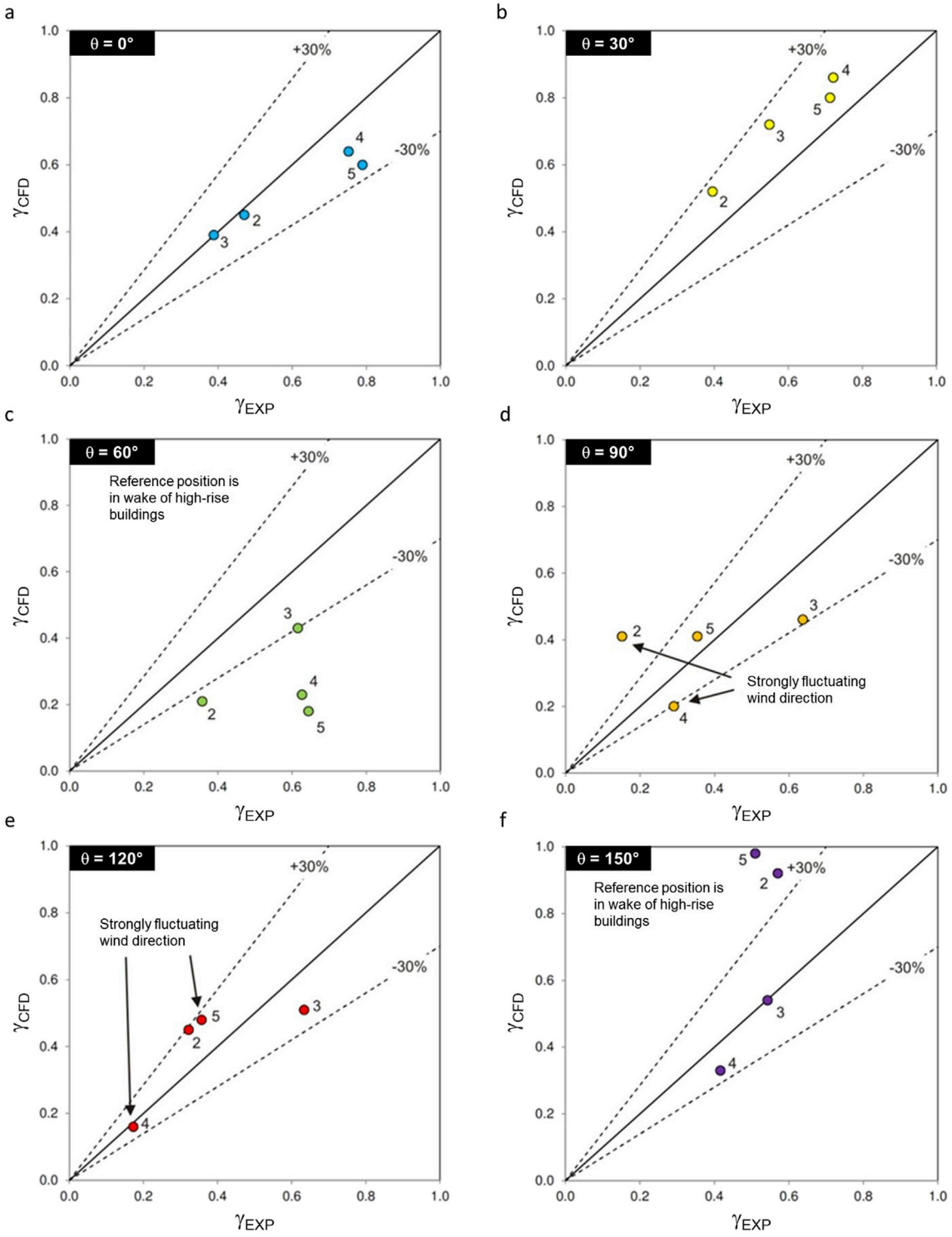

Fig. 8. Computed versus measured wind speed ratios ($\gamma = U/U_{ref}$) for the four near-ground measurement positions and for six reference wind directions (θ).

which causes artificially increased wind speed ratios. The following observations are made:

- Fig. 12a: for $\theta = 0°$, the cruise terminal is partly located in the far wake of upstream buildings. But locally between the cruise ship and the high-rise buildings on the quay, a wind speed-up is observed.
- Fig. 12b: for $\theta = 30°$, the bow of the cruise ship is exposed to the wind approaching over the water, yielding high wind speed ratios near the windward side of the ship.
- Fig. 12c: for $\theta = 60°$, the bow of the cruise ship is also exposed to the wind approaching over the water; however for this wind direction the results are distorted a bit by the fact that the reference position is situated in the wake of nearby high-rise buildings.

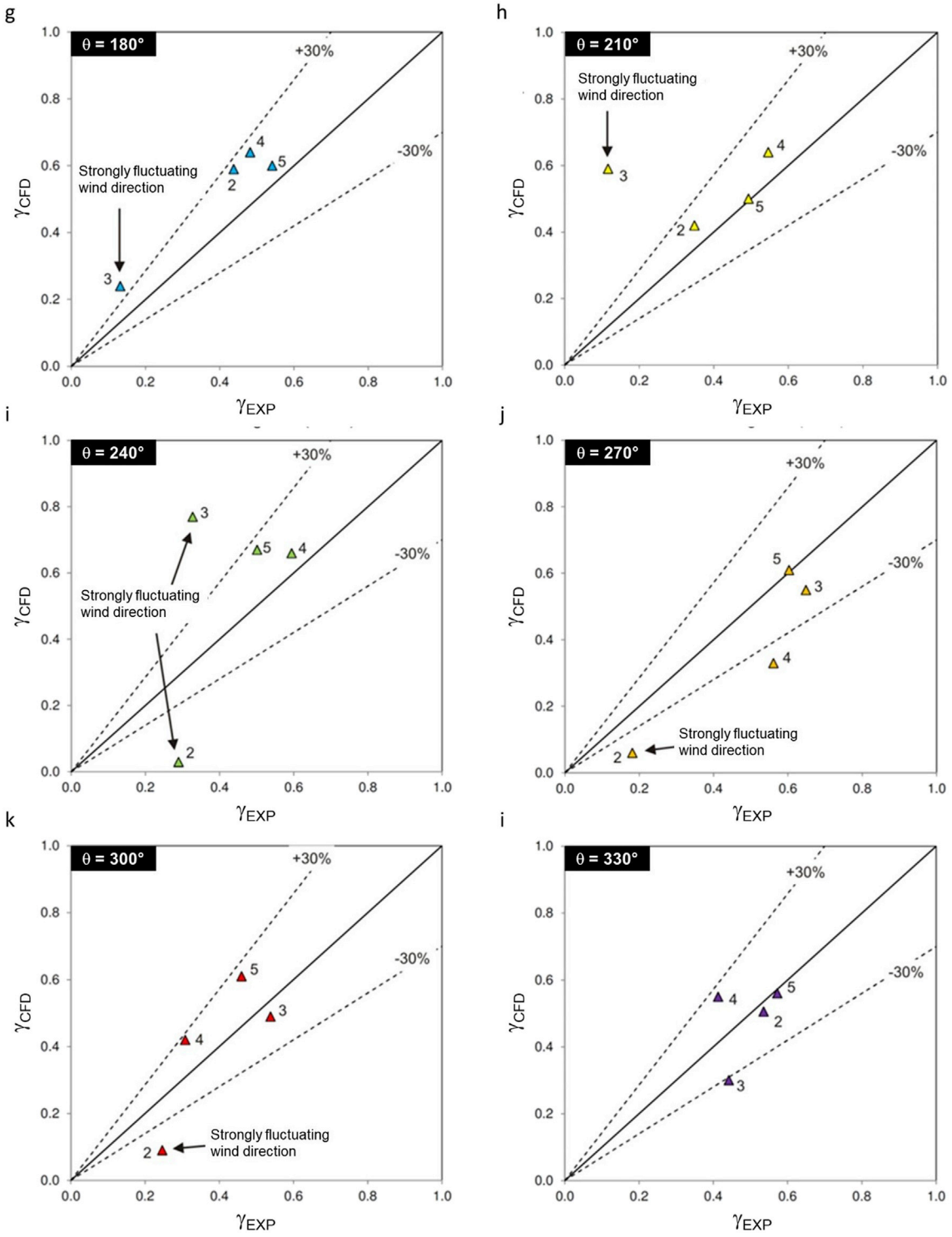

Fig. 9. Computed versus measured wind speed ratios ($\gamma = U/U_{ref}$) for the four near-ground measurement positions and for six reference wind directions (θ).

- Fig. 12d–f: for $\theta = 90°$, $\theta = 120°$, $\theta = 150°$, the cruise ship is largely positioned in the wake of the high-rise buildings on the quay of the Cruise Terminal. Note however that $\theta = 150°$ is a wind direction where again the reference position is in the wake of nearby high-rise buildings.
- Fig. 12g-h: for $\theta = 180°$ and $\theta = 210°$, the cruise ship is still in the wake of nearby high-rise buildings, but at the stern of the ship a clear corner stream (yellow color) can be discerned.
- Fig. 12i: for $\theta = 240°$ the stern of the cruise ship is strongly exposed to the wind approaching over the water.
- Fig. 12j: for $\theta = 270°$, the cruise ship is partly sheltered from wind.
- Fig. 12k-l: for $\theta = 300°$ and $\theta = 330°$, the ship is located upstream of the high-rise buildings on the quay, but also sheltered by the built-up area on the other shore.

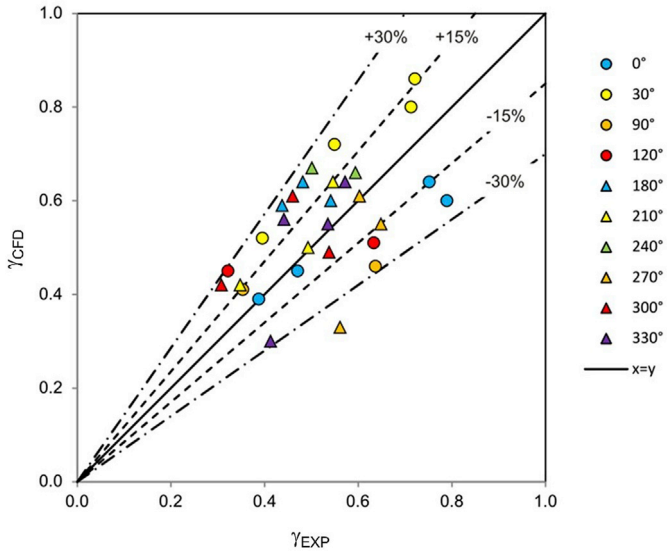

Fig. 10. Computed versus measured wind speed ratios ($\gamma = U/U_{ref}$) for the four near-ground measurement positions and for the twelve reference wind directions (θ), without the data that are clearly disturbed by location of the measurement points situated in the wake of nearly buildings.

5.3. CFD results: pressure coefficients (C_p)

The CFD simulations provide the distribution of the surface pressure on the ship. These results are presented as pressure coefficients (C_P) calculated by Eq. (8):

$$C_P = \frac{(P - P_0)}{\frac{1}{2}\rho U_{ref}^2} \tag{8}$$

where P is the static pressure on the surface, P_0 the reference atmospheric pressure and U_{ref} the mean wind speed at the reference position. Fig. 13 shows the C_P for $\theta = 0°$, $\theta = 120°$ and $\theta = 180°$. The following observations are made by linking the observations in Fig. 13 to those in Fig. 12:

- Figs. 12a and 13a: for $\theta = 0°$, the cruise ship is partly sheltered from wind by the built-up area on the other side of the shore. Fig. 12a shows an increase of wind speed in the passage between the leeward side of the ship and the high-rise buildings on the quay. The windward side indicates C_P values from 0.2 to 0.4 and more. The leeward side of the ship shows near-zero C_P values for the half of the surface near the bow and positive C_P values for the half of the surface near the stern of the ship.
- Figs. 12e and 13b: for $\theta = 120°$, the cruise ship is partly sheltered from wind from the high-rise buildings on the quay. The jet passing between the buildings on the quay impinges on the windward side of the ship yielding C_P values of about 0.5. The bow and the stern are strongly sheltered yielding near-zero C_P values. On the leeward side of the ship, the C_P values are slightly positive, indicating the absence of large flow separation regions around the ship.
- Figs. 12g and 13c: for $\theta = 0°$, the cruise ship is weakly sheltered from wind by the high-rise buildings on the quay. The shelter is only weak because the wind flows through the large passage between the WPC building and the other buildings and impinges fairly directly on the windward side of the ship, yielding C_P values around 0.2. The strong impinging flow yields a strong flow over the ship, and the associated large areas of flow separation over the ship. These in turn yield negative C_P over almost the entire leeward side of the ship.
- Comparing Fig. 13a and b allows to assess the effect of upstream nearby high-rise buildings. The wind directions 0° and 120° represent two fairly symmetrical approach-flow wind directions for the ship, however while there are no nearby high-rise buildings upstream for 0°, such an obstruction is present for 120°. For 0°, the windward side

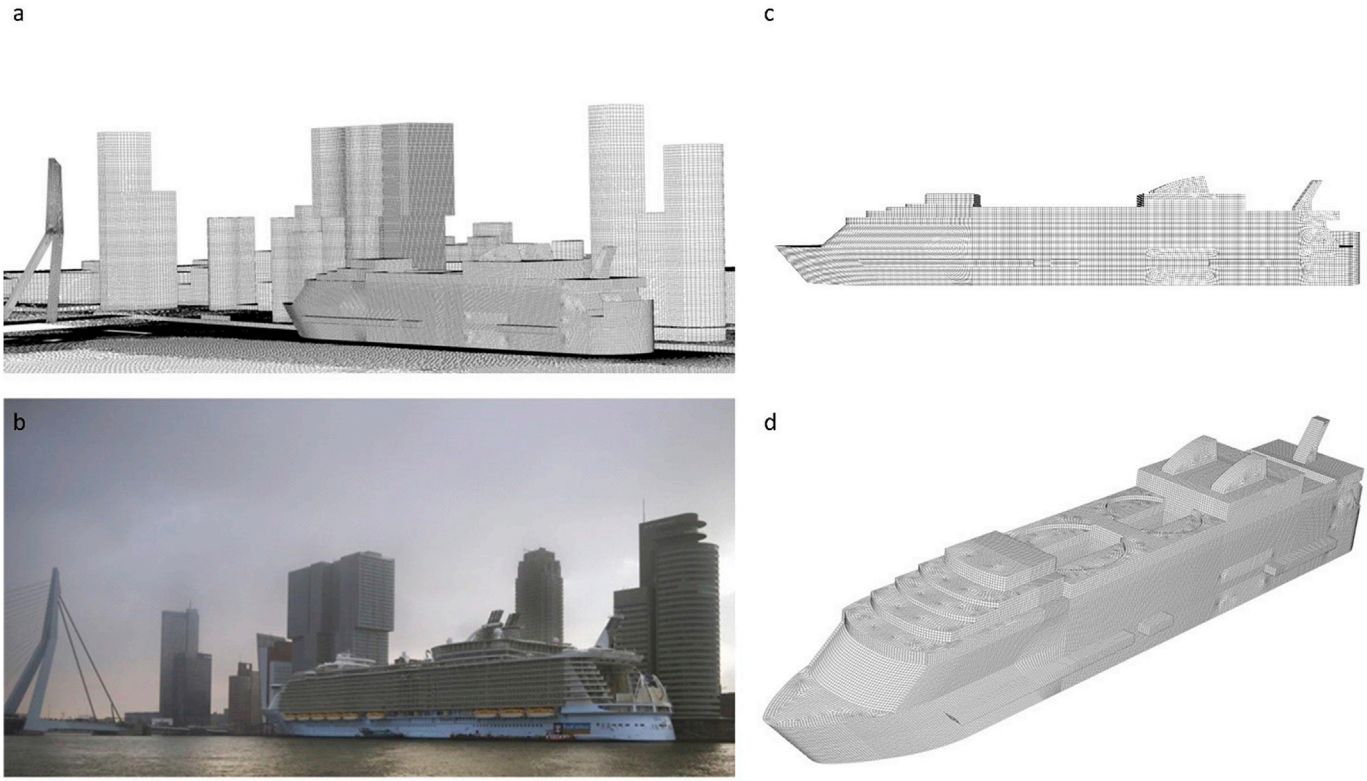

Fig. 11. *(a,b)* Details of computational grid of Cruise Terminal and cruise ship *Oasis of the Seas* and corresponding photograph. (*b*: Source: *NOS.nl*) *(c,d)* Computational grid on the exterior surfaces of the cruise ship. Total cell count (for whole domain) is 58 million.

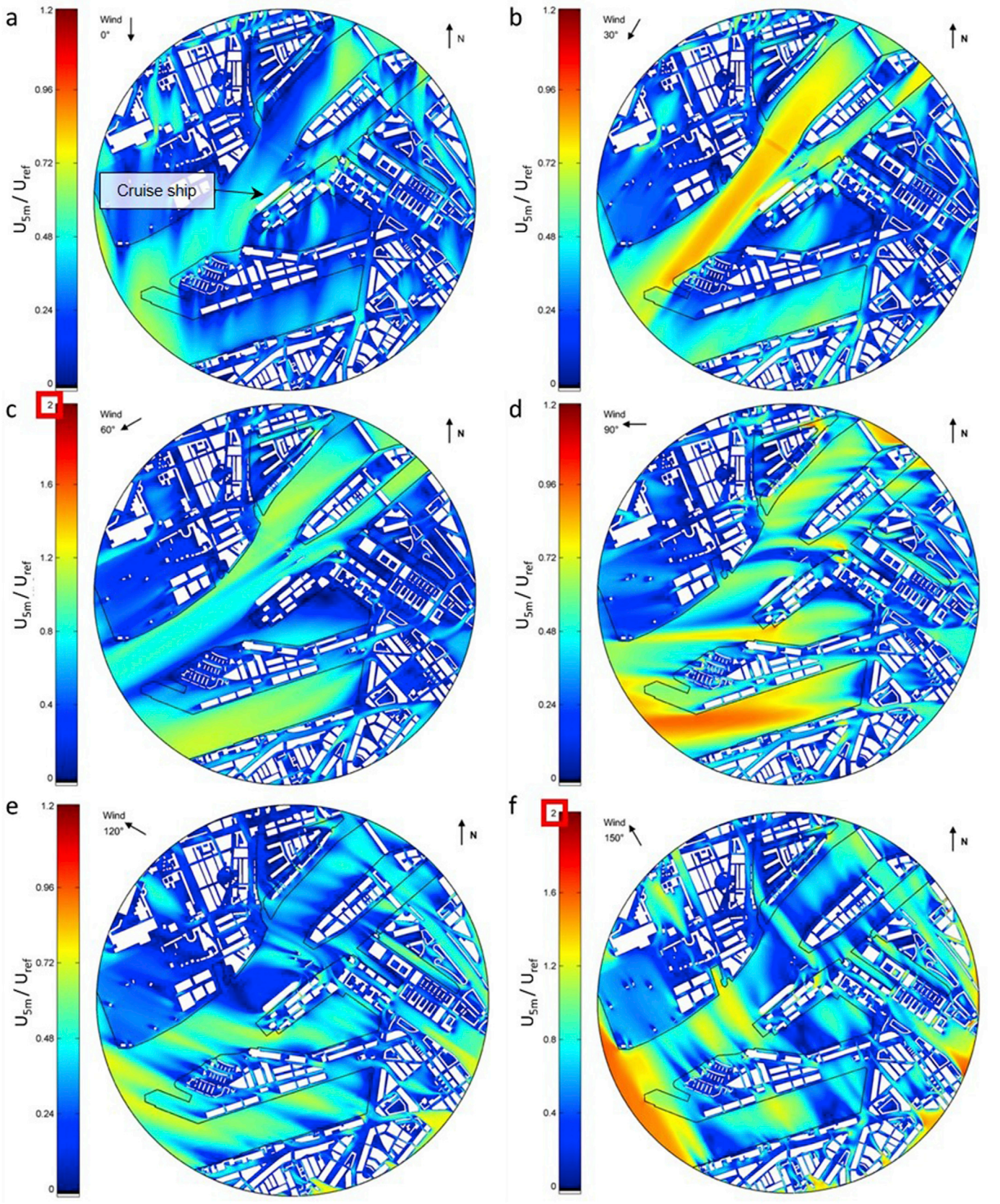

Fig. 12. CFD results: wind speed ratio U_{5m}/U_{ref} in the study area. U_{5m} is the local wind speed at 5 m above NAP. U_{ref} is the wind speed at the reference location on top of the WPC building.

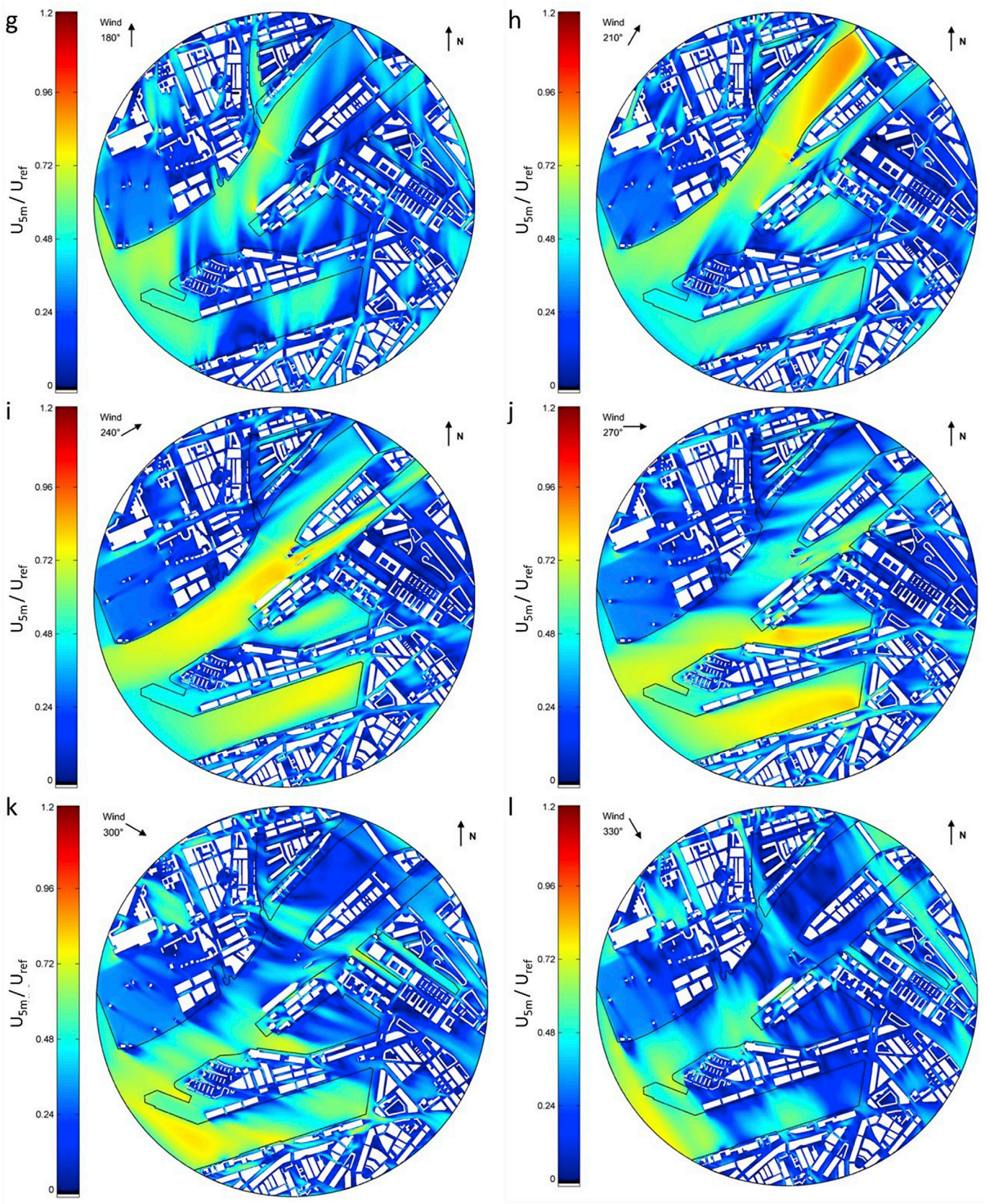

Fig. 12. (*continued*).

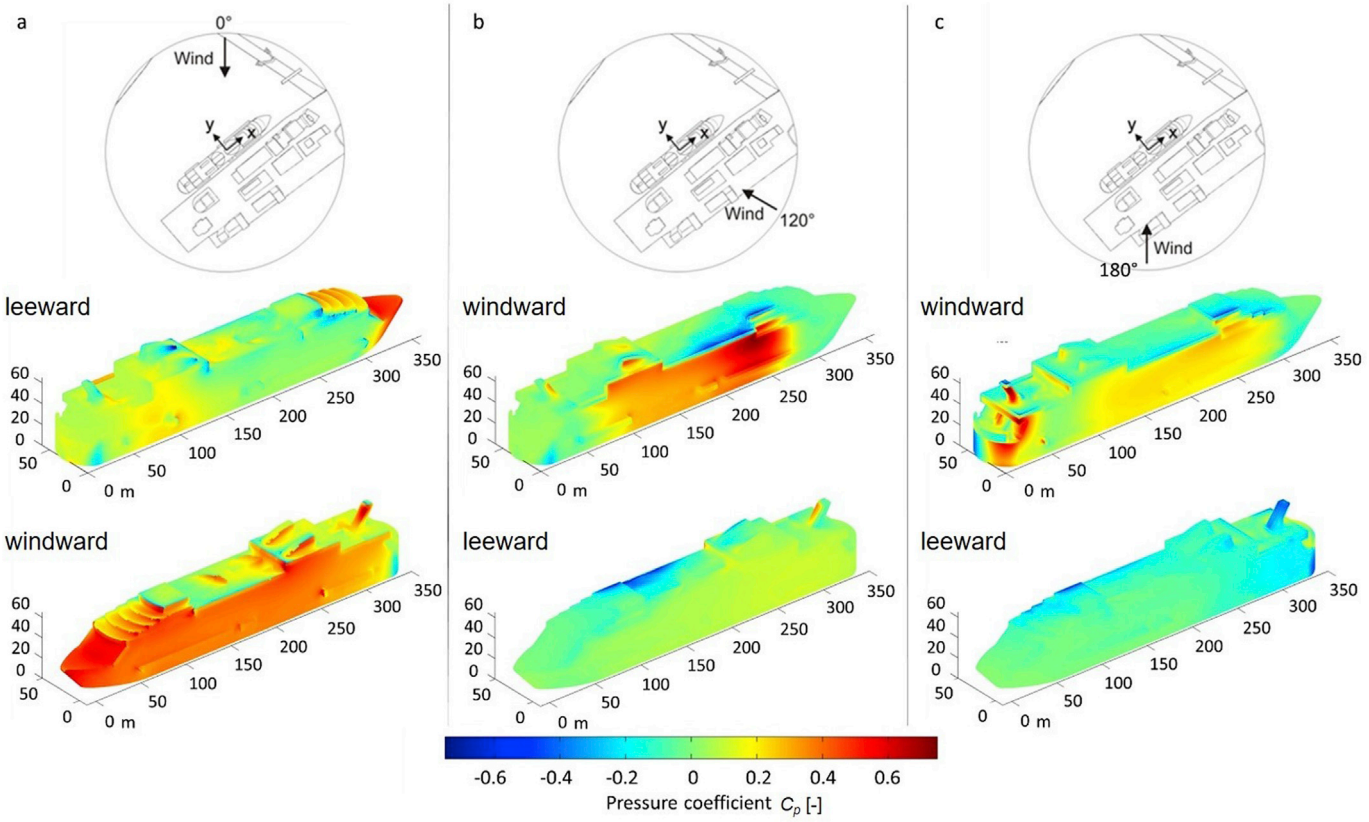

Fig. 13. Mean pressure coefficient C_P on the ship exterior surfaces for three reference wind directions (*a*) $\theta = 0°$, (*b*) $\theta = 120°$ and (*c*) $\theta = 180°$.

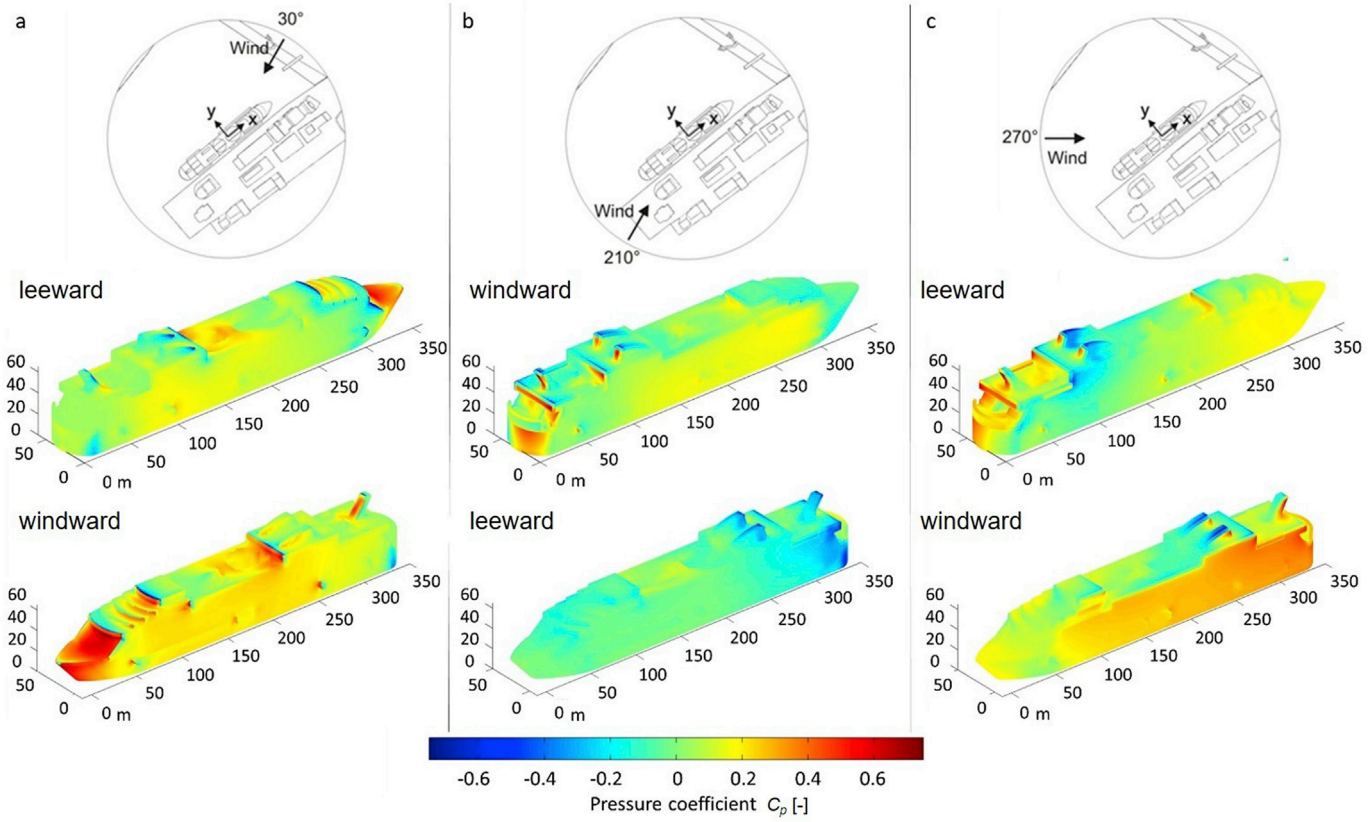

Fig. 14. Mean pressure coefficient C_P on the ship exterior surfaces for three reference wind directions (*a*) $\theta = 30°$, (*b*) $\theta = 210°$ and (*c*) $\theta = 270°$.

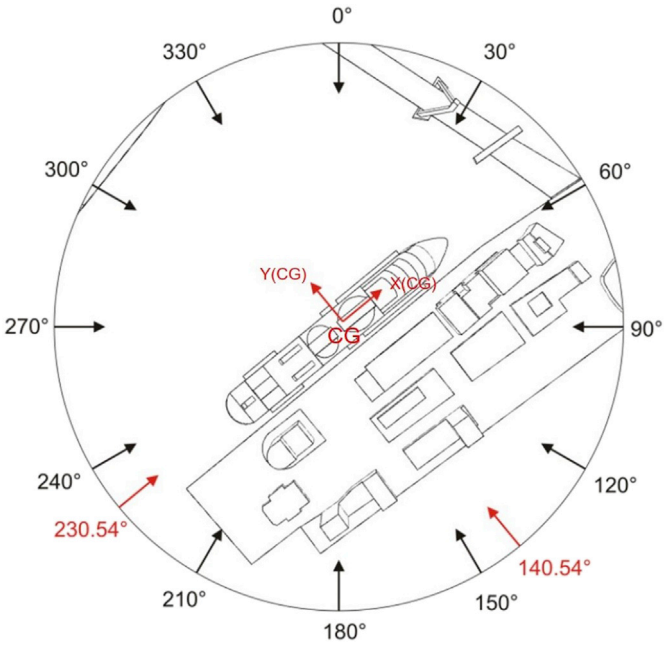

Fig. 15. Indication of reference wind directions (θ) and the center of gravity (CG) of the ship.

of the ship experiences fairly uniform C_P values due to the lack of upstream buildings. For 120°, very large gradients are present. Comparing Fig. 13a and b, it is clear that locally the largest C_P values occur for the position with high-rise buildings upstream. These buildings clearly lead to locally amplified surface pressure compared to the case without high-rise buildings upstream.

Fig. 14 shows the C_P for $\theta = 30°$, $\theta = 210°$ and $\theta = 270°$. The following observations are made:

- Figs. 12b and 14a: for $\theta = 30°$, the bow of the cruise ship is exposed to the wind approaching over the water, yielding high wind speed ratios near the windward side of the cruise ship. The C_P values are large at the stern, and quite uniform and positive on the windward side. On the leeward side of the ship, there are some zones with negative C_P near the stern and the bow, but generally the C_P is quite uniform and positive.
- Figs. 12h and 14b: for $\theta = 210°$, the cruise ship is still in the wake of nearby high-rise buildings, but at the stern of the ship a clear corner stream (yellow color) can be discerned. On the windward side of the ship, a C_P distribution is found with overall positive values, albeit with locally negative values near the bow and the stern. On the leeward side, the strong corner stream near the stern leads to negative C_P on the surface near the stern.
- Figs. 12j and 14c: for $\theta = 270°$, the cruise ship is partly sheltered from wind by distant upstream buildings. The C_P values on the windward side are generally positive, with larger values found at the stern than the bow. On the leeward side, the C_P varies in a range of about - 0.2 (at the stern) and +0.2 (at the bow).
- Comparing Fig. 14b and c allows to assess the effect of upstream nearby high-rise buildings. The wind directions 210° and 270° represent two fairly symmetrical approach-flow wind directions for the ship, however while there are no nearby high-rise buildings upstream for 270°, such an obstruction is present for 210°. For 270°, the windward side of the ship experiences high C_P values, up to about 0.4, as opposed to 210°. For 210°, the C_P gradients across the windward surface are much larger, especially near the bow and the stern. On the

Table 2
Center of pressure (CoP) for the wind forces on the cruise ship *Oasis of the Seas* calculated with respect to the local reference system (x,y,z) of Figs. 16 and 17.

reference wind direction	x [m]	y [m]	z [m]
0°	190.1	0	29.5
30°	223.1	0	32.1
60°	195.8	0	21.4
90°	177.5	0	21.8
120°	188.2	0	22.8
150°	163.9	0	22.8
180°	125.2	0	21.0
210°	119.6	0	21.7
240°	1307.7*	0*	−15.3*
270°	101.7	0	28.8
300°	156.2	0	29.8
330°	178.6	0	28.7

*Center of pressure is situated outside the volume of the ship.

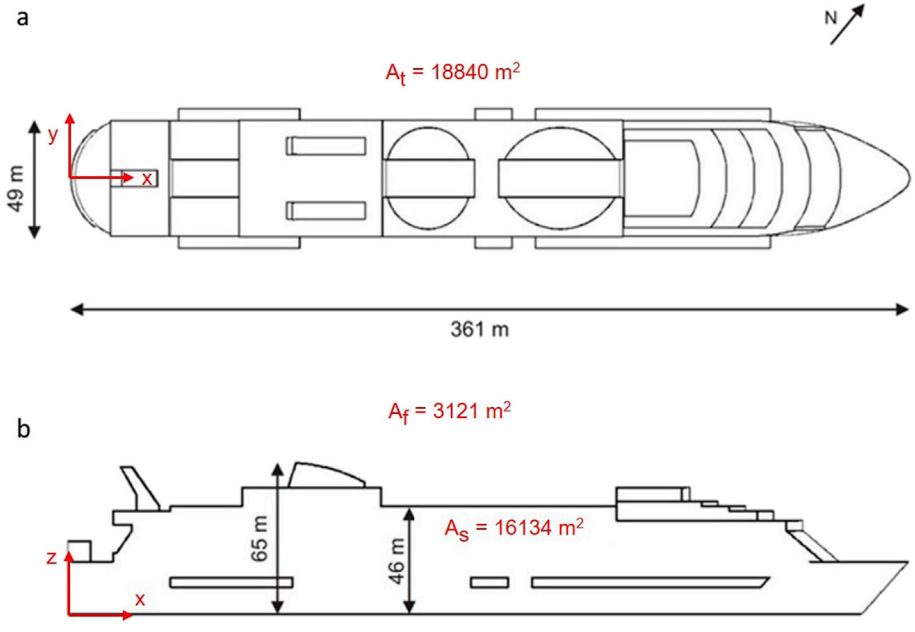

Fig. 16. (*a,b*) Local reference system, main ship dimensions, projected areas A_t (top), A_s (side) and A_f (frontal).

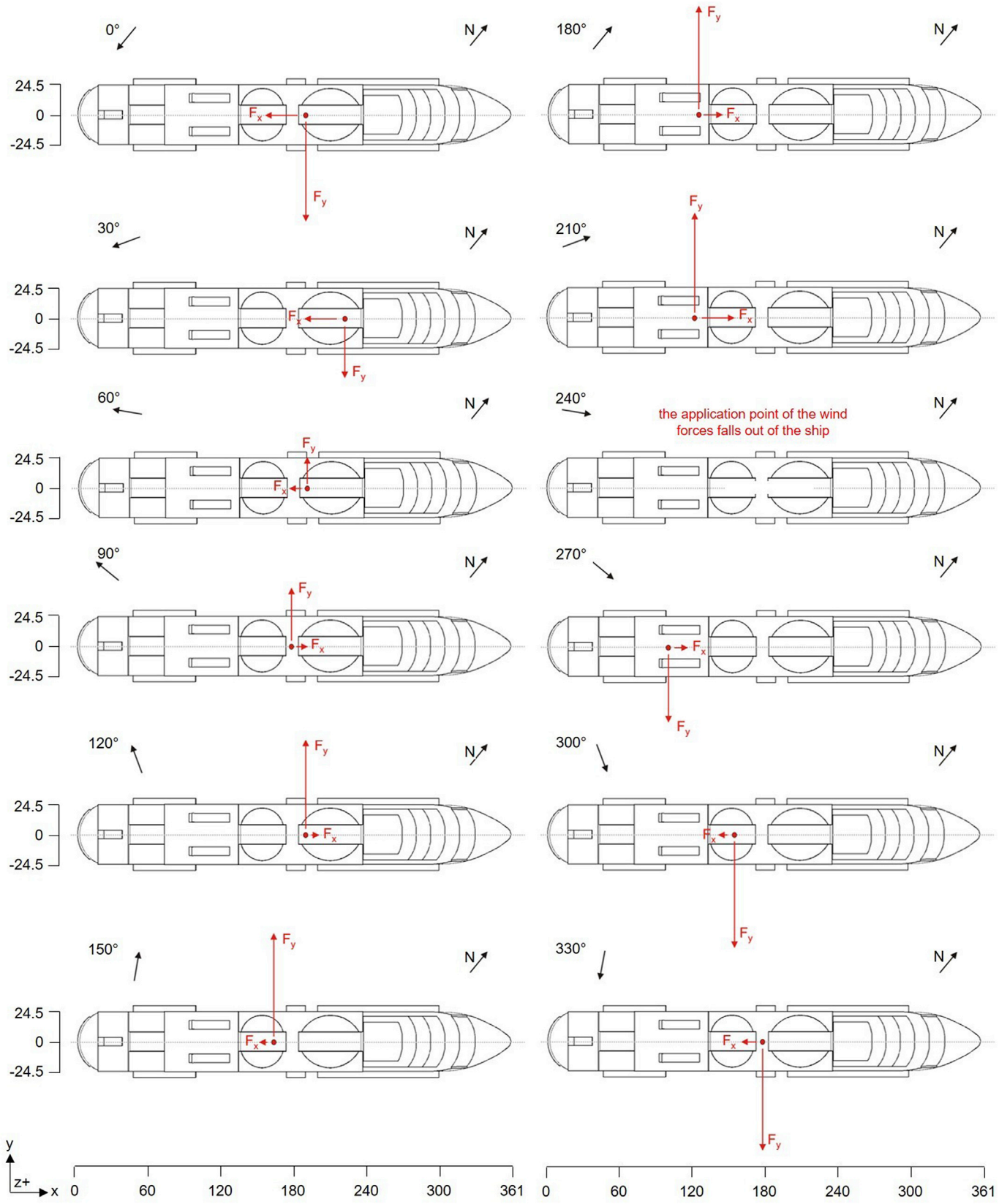

Fig. 17. Center of pressure (CoP) of the wind forces on the cruise ship *Oasis of the Seas* for all reference wind directions (θ) analyzed.

Table 3
CFD results of force coefficients on the cruise ship *Oasis of the Seas*.

reference wind direction	C_X [-]	C_Y [-]	C_Z [-]
0°	−0.35	−0.25	0.09
30°	−0.46	−0.14	0.12
60°	−0.18*	0.14*	0.08*
90°	0.10	0.19	0.24
120°	0.01	0.19	0.26
150°	−0.42*	1.02*	1.03*
180°	0.27	0.28	0.21
210°	0.33	0.19	0.08
240°	0.43	0.00	0.00
270°	0.20	−0.19	−0.03
300°	−0.06	−0.37	0.11
330°	−0.26	−0.34	0.09

*Reference position in wake of nearby high-rise buildings.

leeward side of the ship, large C_P gradients are found across the surface for 270° with both positive and negative C_P. For 210°, almost the entire leeward surface experiences negative C_P.

5.4. CFD results: wind forces

Wind forces on the ship *Oasis of the Seas* moored at the quay of the Cruise Terminal of Rotterdam Port are calculated in the dimensionless form using Eqs. (2)–(4) (Fig. 15). The velocity reference U_{ref} is taken in the computational domain at position 1, i.e. the reference position on the roof of the WPC building. . The projected front area ($A_f = 3121$ m^2), the projected side area ($A_s = 16134$ m^2) and the projected top area ($A_t = 18840$ m^2) of the ship are considered in the above-mentioned equations (Fig. 16). Table 2 and Fig. 17 show the results, with the forces indicated in the center of pressure (CoP). The CoP is always located on the ship except for wind direction $\theta = 240°$ (Fig. 17 and Table 2). For this reference wind direction the wind blows on the stern of *Oasis of the Seas* and forces are minimal with respect to other wind directions where the lateral sides of the ship were completely exposed to the wind (see Fig. 12). It may be concluded that for this wind direction no tugboats are needed. However, for its full route to the port, the ship direction will not always be parallel to the wind direction and in this scenario the wind could strongly push the ship towards the quay, as clearly happened to the MS Nordnorge at the Port of Bodo, Norway (Corriere della Sera, 2020; Alexander Farstad). Note that the forces coefficients for $\theta = 60°$ and $\theta = 150°$ may be distorted by the deficiencies of the reference position that is in the wake of upstream buildings for these particular two wind directions (Table 3). Nevertheless, all these coefficients can be used in combination with the measurements at the reference position to determine the expected forces on the ship and to determine the berth requirements such as safe working loads of bollards and fenders.

To assess the influence of upstream nearby high-rise buildings, similar to subsection 5.3, we compare the side and vertical force coefficients (C_Y, C_Z) for $\theta = 0°$ versus $\theta = 120°$ and those for $\theta = 210°$ versus $\theta = 270°$. For $\theta = 0°$, the absolute value of C_Y (= −0.25) is larger than for 120° (0.19). The net result of the buildings on the ship is to provide some shelter, even though the highest C_P on the ship's surface is found for the sheltered case ($\theta = 120°$). For $\theta = 210°$, C_Z (= 0.26) is much larger than for 0° ($C_Z = 0.09$), indicating that the upstream buildings increase the upward force (Table 3).

For both $\theta = 210°$ and $\theta = 270°$, $C_Y = 0.19$. As shown in Fig. 14, the surface pressures on the windward and the leeward side however are very different. For $\theta = 270°$, without nearby upstream high-rise buildings, there is large positive C_P on the windward side versus a near-zero or slightly positive C_P on the leeward side. For $\theta = 210°$, with nearby upstream high-rise buildings, the buildings reduce the magnitude of C_P on the windward side and lead to more negative C_P on the leeward side. For C_Z, the absolute differences are limited ($C_Z = 0.08$ for $\theta = 210°$ versus C_Z = - 0.03 for $\theta = 270°$) although also here the presence of the upstream buildings leads to a larger positive (i.e. upward) force (Table 3). This can be attributed to the fact that the highest wind speed amplification around high-rise buildings occurs near ground level at the pedestrian level (see e.g. Blocken et al., 2007b, 2008 for velocity profiles as a function of height in passages between buildings), and that this flow impinges at the bottom of the windward side of the ship and is then deviated upwards along the ship's surface.

While the coefficient C_Y was found to decrease by the presence of nearby buildings (Table 3), the locally amplified C_P on a large part of the ship surface in Fig. 14b indicates that for smaller ships, the net horizontal force can increase due to the presence of nearby upstream buildings. Further research is required to analyze situations with different types of ships and different types of buildings and building groups on the quay.

6. Summary and conclusions

A nautical port is usually an aerodynamically complex built-up area with large spatial changes in aerodynamic roughness length and significant local temporal changes in geometry by the presence of large ships. The wind forces on ships in ports can be very different from those on ships at open sea. Over the past decades, ships have been getting larger and larger while port layout has mainly remained the same. This increase in ship size as been observed both for container ships and cruise ships. Cruise ships and container ships are similar in that they are both characterized by large overall sizes but also by the fact that the majority of the ship's lateral surfaces are situated above the waterline, yielding a large windage area, which increases the contribution of the wind loads to the total loads on the ship. As an example, the cruise ship the *Oasis of the Seas* has a height of 65 m above the water line and a depth of 22.55 m.

The increasing ship size has raised the need for more precise knowledge about the wind forces on a ship in the port. Such knowledge is required to fine-tune the admission policy of the port. It is also required for the (tugboat) pilots as it provides them and the simulation institutes with the necessary data for safely maneuvering the ship and for building accurate mathematical models for maneuvering simulators. Pilots and tugboat captains follow training courses which make use of dedicated maneuvering simulators. Finally, the knowledge of wind forces on the ships in the port area is necessary for determining the berth requirements such as safe working loads of bollards and fenders.

This paper has presented a case study in which the wind forces on a large cruise ship, the *Oasis of the Seas*, moored at the quay of the Rotterdam Cruise Terminal are determined. The Cruise Terminal quay contains several high-rise buildings which can substantially influence the wind loads on the ship. CFD simulations based on the 3D steady RANS equations are used to obtain the wind velocity field, surface pressure distributions and the resulting wind forces. Wind speeds and wind directions are validated by on-site measurements carried out for the same area. The wind forces exerted on the *Oasis of the Seas* are evaluated by the RANS simulations. A previous study by Janssen et al. (2017), in which wind forces on a container ship in open sea-like conditions were determined by 3D steady RANS simulations and validated by WT tests (by Andersen, 2013), was also reported here. This study guided the level of geometrical simplification for the cruise ship *Oasis of the Seas* and indicated the computational settings and parameters required to obtain accurate simulation results. Although this study focused on wind forces on a ship moored at a quay of the port of a particular European city, the same methodology can be applied to different scenarios worldwide. For instance, ships approaching the entrance of a port, ships crossing sea locks inside a port area, or simply ships navigating through a narrow canal inside cities can experience strong local wind conditions which may lead to unsafe conditions.

The study has shown that the presence of nearby upstream high-rise buildings generally increases the gradients in surface pressure over the ship's surface. The presence of the high-rise buildings can yield locally amplified surface pressure, but due to the size of the ship, it has been found that the net horizontal force decreases. This is due to the fact that the ship's length is much larger than the width of the buildings, by which

some parts of the ship's lateral surface are sheltered, while others are more exposed. For smaller ships, nearby high-rise buildings can yield increased or decreased horizontal lateral forces, depending on the wind direction and the relative position of ship and buildings. However, for the *Oasis of the Seas*, it was found that the net vertical upward force increases. This can be attributed to the fact that the highest wind speed amplification around high-rise buildings occurs around the buildings near ground level (pedestrian level) and that this flow impinges at the bottom of the windward side of the ship and is then deviated upwards along the ship's surface.

High-quality grid generation and CFD simulations for such a large area as in this study is rather time-consuming. Undoubtedly, WT experiments would have been faster. Nevertheless, CFD was considered as the most suitable method for the present case study, for several reasons. WT tests on such a large area would only have been feasible in WTs with very wide test sections, in order to avoid using too large geometrical scaling factors and violating similarity requirements too much. Even though WT tests of wind forces on the cruise ship would probably have been more accurate than the results of the CFD simulations, the CFD simulation results provided more insight into the relationship between the complicated wind-flow pattern around the ship and the nearby buildings and the resulting forces on the ship (Blocken, 2014).

In conclusion, the fact that cruise ships often moor in ports inside the built environment and that the presence of high-rise buildings can strongly influence the wind forces, requires dedicated research to ensure safe navigating and mooring.

CRediT authorship contribution statement

A. Ricci: Writing, data analysis, data and text editing, revising. **W.D. Janssen:** Numerical and experimental investigations, data analysis, reporting, revising. **H.J. van Wijhe:** Funding acquisition, supervision, revising. **B. Blocken:** Funding acquisition, supervision, writing, data and text editing, revising.

Declaration of competing interest

The authors declare that they have no known competing financial interests or personal relationships that could have appeared to influence the work reported in this paper.

Acknowledgements

This project was initiated by the Port of Rotterdam (H.J. van Wijhe) and executed by Eindhoven University of Technology (TU/e) to improve the accessibility of the port and the efficiency and safety of the port operations. TU/e acknowledges the Port of Rotterdam for the fruitful collaboration. The authors also acknowledge the partnership with ANSYS CFD.

References

Aage, C., 1968. Vindkræfter På Skibe (WindforcesonShips). Institut for Skibs-og Havteknik, Danmarks Tekniske Højskole.
Aage, C., Hvid, S.L., Hughes, P.H., Leer-Andersen, M., 1997. Wind loads on ships and offshore structures estimated by CFD. In: Proceedings of the 8th International Conference on the Behaviour of Offshore Structures, vol. 97. BOSS.
Andersen, I.M.V., 2013. Wind loads on a post-panamax container ship. Ocean. Eng. 58, 115–134.
Andersson, G.O., 1978. Untersuchung der Fahrtverluste durch Wind und Seegang bei einem schnellen Einschrauben-Containerschiff (Investigation of the Speed Loss in Wind and Seaway of a Fast Single Screw Container Ship). Bundesministerium fur Forschung und Technologie, Meerestechnik.
ANSYS Fluent, 2013. Release 15.0, Theory Guide. ANSYS Inc, Canonsburg.
Baker, C.J., 2007. Wind engineering - past, present and future. J. Wind Eng. Ind. Aerod. 95, 843–870.
Bardera Mora, R., 2014. Experimental investigation of the flow on a simple frigate shape (SFS). Sci. World J. 2014 article ID 818132.
Benham, F.A., 1977. Prediction of Wind and Current Loads on VLCC's. Oil companies International Marine Forum, London, England.
Blendermann, W., 1994. Parameter-identification of wind loads on ships. J. Wind Eng. Ind. Aerod. 51 (3), 339–351.
Blendermann, W., 1995. Estimation of wind loads on ships in wind with a strong gradient. I-A Proceedings of the 14th International Conference on Offshore Mechanics and Arctic Engineering (OMAE1995, 271–277.
Blendermann, W., 1997. Messung der Windlast an zwei Containerschiffen in realem Ladezustand im Windkanal (Measurements of the Wind Loads on two Container Ships in Real Loading Conditions in Wind Tunnel). Institut für Schiffbau der Universität Hamburg.
Blocken, B., 2014. 50 years of computational wind engineering: past, present and future. J. Wind Eng. Ind. Aerod. 129, 69–102.
Blocken, B., 2015. Computational Fluid Dynamics for Urban Physics: importance, scales, possibilities, limitations and ten tips and tricks towards accurate and reliable simulations. Build. Environ. 91, 219–245.
Blocken, B., 2018. LES over RANS in building simulation for outdoor and indoor applications: a foregone conclusion? Building Simulation 11 (5), 821–870.
Blocken, B., Persoon, J., 2009. Pedestrian wind comfort around a large football stadium in an urban environment: CFD simulation, validation and application of the new Dutch wind nuisance standard. J. Wind Eng. Ind. Aerod. 97 (5–6), 255–270.
Blocken, B., Stathopoulos, T., Carmeliet, J., 2007a. CFD simulation of the atmospheric boundary layer: wall function problems. Atmos. Environ. 41 (2), 238–252.
Blocken, B., Carmeliet, J., Stathopoulos, T., 2007b. CFD evaluation of the wind speed conditions in passages between buildings – effect of wall-function roughness modifications on the atmospheric boundary layer flow. J. Wind Eng. Ind. Aerod. 95 (9–11), 941–962.
Blocken, B., Moonen, P., Stathopoulos, T., Carmeliet, J., 2008. A numerical study on the existence of the Venturi-effect in passages between perpendicular buildings. Journal of Engineering Mechanics - ASCE 134 (12), 1021–1028.
Blocken, B., van der Hout, A., Dekker, J., Weiler, O., 2015. CFD simulation of wind flow over natural complex terrain: case study with validation by field measurements for Ria de Ferrol, Galicia, Spain. J. Wind Eng. Ind. Aerod. 147, 43–57.
Britter, R., Schatzmann, M., 2007. Model Evaluation Guidance and Protocol Document COST Action 732. COST Office Brussels, Belgium, ISBN 3-00-018312- 4.
Brizzolara, S., Rizzuto, E., 2006. Wind heeling moments on very large ships-some insights through cfd results. STAB 9th International Conference on Stability of Ships and Ocean Vehicles. Rio De Janeiro, Brasil.
Bucci, V., Marino, A., Mauro, F., Nabergoj, R., Nasso, C., 2016. In: Zolotarev, I., Radolf, V. (Eds.), On Advanced Ship Evacuation Analysis. Engineering Mechanics 2016, pp. 98–101. Engineering Mechanics.
Burlando, M., Pizzo, M., Repetto, M.P., Solari, G., De Gaetano, P., Tizzi, M., 2014. Short-term wind forecast for the safety management of complex areas during hazardous wind events. J. Wind Eng. Ind. Aerod. 135, 170–181.
Carpentieri, M., Robins, A.G., 2015. Influence of urban morphology on air flow over building arrays. J. Wind Eng. Ind. Aerod. 145, 61–74.
Casey, M., Wintergerste, T., 2000. Best Practice Guidelines, ERCOFTAC Special Interest Group on Quality and Trust in Industrial CFD. ERCOFTAC, Brussels.
Castillo-Manzano, J.I., Lopez-Valpuesta, L., 2018. What does cruise passengers' satisfaction depend on? Does size really matter? Int. J. Hospit. Manag. 75, 116–118.
Cebeci, T., Bradshaw, P., 1977. Momentum Transfer in Boundary Layers. Hemisphere Publishing Corporation, New York.
Corriere della Sera, 2020. Alexander Farstad. URL: https://video.corriere.it/norvegia-traghetto-travolto-tempesta-colpisce-muretto-molo/9403967c-429a-11ea-8fab-5eae1fe9ccd1 (day of the event: 29.01.2020).
Crudu, L., Obreja, D.C., Pacuraru, S., 2016. Evaluation of influences of wind induced forces and moments on the resistance and maneuverability of river ships. Proceedings of the Third International Conference on Traffic and Transport Engineering (ICTTE) 250–259.
Wnęk, A.D., Guedes Soares, C., 2015. CFD assessment of the wind loads on an LNG carrier and floating platform models. Ocean. Eng. 97, 30–36.
DNVVessel Register, GL, 2019. Oasis of the Seas: Dimensions (27091). Det Norske Veritas. Retrieved 28. (Accessed December 2019).
Engineering Sciences Data Unit (ESDU) 80024, 1980. Blockage Corrections for Bluff Bodies in Confined Flows. ESDU International PLC.
Maritime Executive, 2017. Container Ship Breaks Loose in Boston Harbor. URL: https://www.maritime-executive.com/article/container-ship-breaks-loose-in-boston-harbor (day of the event: 12.07.2017).
Ferziger, J.H., Perić, M., 2002. Computational Methods for Fluid Dynamics, third ed. Springer-Verlag, ISBN 3-540-42074-6.
Flows Magazine, 2019. APL Mexico City Antwerpen. URL: https://www.youtube.com/watch?v=6uz9SEou3Ig (day of the event: 09.12.2019).
Franke, J., Hellsten, A., Schlünzen, H., Carissimo, B., 2007. Best Practice Guideline for the CFD Simulation of Flows in the Urban environment. COST Action 732: Quality Assurance and Improvement of Microscale Meteorological Models.
Fujiwara, T., Nimura, T., 2005. New estimation method of wind forces acting on ships on the basis of mathematical model. International Offshore and Polar Engineering Conference Proceedings 3, 82–89.
Fujiwara, T., Tsukada, Y., Kitamura, F., Sawada, H., 2009. Experimental investigation and estimation on wind forces for a container ship. Summaries of Papers Published by Staff of National Maritime Research Institute at Outside Organizations 9.
Gomez Paz, M.A., Camarero Orive, A., Gonzalez Cancelas, N., 2015. Use of the Delphi method to determine the constraints that affect the future size of large container ships. Marit. Pol. Manag. 42 (3), 263–277.
Gould, R.W.F., 1967. Measurements of the Wind Forces on a Series of Models of Merchant Ships. Aerodynamics Division, Teddington, vol. 1233. National Physical Laboratory, U. K. Aero Report.

The Guardian, 2019. The Guardian News. Cruise ship crashes into Venice dock. URL: https://www.youtube.com/watch?v=GyCLhvxpQt0 (day of the event: 02.06.2019).
Haddara, M.R., Guedes Soares, C., 1999. Wind loads on marine structures. Mar. Struct. 12, 199–209.
Hang, J., Chen, L., Lin, Y., Buccolieri, R., Lin, B., 2018. The impact of semi-open settings on ventilation in idealized building arrays. Urban Climate 25, 196–217.
Hanjalic, K., 2005. Will RANS survive LES? A view of perspectives. J. Fluid Eng. 127, 831–839.
Hong, B.G., 1991. A method of calculating the wind coefficient of ships. J Dalian Mar College 2, 113–121.
Hughes, G., 1930. Model Experiments on the Wind Resistance of Ships, vol. 72. Institution of Naval Architects, Transactions, pp. 310–325 discussion.
Hughes, G., 1932. The air resistance of ship's hulls with various types and distributions of superstructure. Inst. E.&S., Scot. 75, 302.
Isherwood, R.M., 1972. Wind Resistance of Merchant Ships, vol. 1. Royal Institution of Naval Architects, England, pp. 327–338, 14.
Janssen, W.D., Blocken, B., van Wijhe, H.J., 2017. CFD simulations of wind loads on a container ship: validation and impact of geometrical simplifications. J. Wind Eng. Ind. Aerod. 166, 106–116.
Koop, A., Rossin, B., Vaz, G., 2012. Predicting Wind Loads on Typical Offshore Vessels Using CFD. In: Proceeding of the ASME 2012 31st International Conference on Ocean, Offshore and Artic Engineering (OMAE2012). Rio de Janeiro, , Brazil. July 1-6, 2012.
La Sicilia. La Sicilia. URL: https://www.youtube.com/watch?v=GJtVt4oKiFc&t=7s (day of the event: 08.07.2019).
Launder, B.E., Spalding, D.B., 1974. The numerical computation of turbulent flows. Comput. Methods Appl. Mech. Eng. 3, 269–289.
Lu, H.A., Yeh, J., 2019. The impact of using mega containerships on operation and management of Shipping Lines. Transport. J. 58 (1), 38–64.
Malchow, U., 2017. Growth in containership sizes to be stopped? Maritime Business Review 2 (3), 199–210.
Martin, J., Martin, S., Pettit, S., 2015. Container ship size and the implications on port call workload. Int. J. Shipp. Transp. Logist. (IJSTL) 7 (5), 553–569.
Merk, O., 2015. The Impact of Mega-Ships. OECD-Report.
Ministry of Defence, 2020. URL: https://english.defensie.nl/topics/hydrography/coordinate-systems-at-sea/coordinate-reference-systems-for-depth-measurement-at-sea.
Mutimer, G.R., 1955. Wind-tunnel tests to determine aerodynamic forces and moments on ships at zero heel. David Taylor Naval Ship Research and Development Center. Report 956, Aero Data Report 27.
DutchNews.nl, 2018. Reformatorisch Dagblad. Noah's ark breaks free as storm batters Dutch fishing village. URL: https://www.youtube.com/watch?v=fFmaPGhC1vI&feature=emb_title (day of the event: 03.01.2018).
OCIMF, 1994. Prediction of Wind Loads and Current Loads on VLCCs.
Ocimf, Sigtto, 1985. Prediction of Wind Loads on Large Liquefied Gas Carriers. Hyperion Books.
Owens, R., Palo, P., 1982. Wind-induced Steady Loads on ships. Naval Civil Engineering Laboratory Port Hueneme, California, p. 93043. Technical Note.
Pasquill, F., 1961. The estimation of the dispersion of windborne material. Meteorol. Mag. 90, 33–49.
Paulauskas, V., Paulauskas, D., Wijffels, J., 2009. Ship safety in open ports. Transport 24 (2), 113–120.
Port of Rotterdam, 2020. URL: https://www.portofrotterdam.com/nl/onze-haven/feiten-en-cijfers/feiten-en-cijfers-over-de-haven/haveninfrastructuur (accessed: 16.07.2020).
Repetto, M.P., Burlando, M., Solari, G., De Gaetano, P., Pizzo, M., 2017. Integrated tools for improving the resilience of seaports under extreme wind events. Sustainable Cities and Society 32, 277–294.
Repetto, M.P., Burlando, M., Solari, G., De Gaetano, P., Pizzo, M., Tizzi, M., 2018. A web-based GIS platform for the safe management and risk assessment of complex structural and infrastructural systems exposed to wind. Advanced in Engineering Software 117, 29–45.
Ricci, A., Kalkman, I., Blocken, B., Burlando, M., Freda, A., Repetto, M.P., 2017a. Local-scale forcing effects on wind flows in an urban environment: impact of geometrical simplifications. J. Wind Eng. Ind. Aerod. 170, 238–255.
Ricci, A., Burlando, M., Freda, A., Repetto, M.P., 2017b. Wind tunnel measurements of the urban boundary layer development over a historical district in Italy. Build. Environ. 111, 192–206.
Ricci, A., Kalkman, I., Blocken, B., Burlando, M., Freda, A., Repetto, M.P., 2018. Large-scale forcing effects on wind flows in the urban canopy: impact of inflow conditions. Sustainable cities and Society 42, 593–610.
Ricci, A., Burlando, M., Repetto, M.P., Blocken, B., 2019. Simulation of urban boundary and canopy layer flows in port areas induced by different marine boundary layer inflow conditions. Sci. Total Environ. 670, 876–892.
Ricci, A., Kalkman, I., Blocken, B., Burlando, M., Repetto, M.P., 2020. Impact of turbulence models and roughness height in 3D steady RANS simulations of wind flow in an urban environment. Build. Environ. 171, 106617.
Richards, P.J., Hoxey, R.P., 1993. Appropriate boundary conditions for computational wind engineering models using the k-ε turbulence model. J. Wind Eng. Ind. Aerod. 46–47, 145–153.
Roubos, A., Groenewegen, L., Peters, D.J., 2017. Berthing velocity of large seagoing vessels in the port of Rotterdam. Mar. Struct. 51, 202–219.
Roubos, A., Peters, D.J., Groenewegen, L., Steenbergen, R., 2018. Partial safety factors for berthing velocity and loads on marine structures. Mar. Struct. 58, 73–91.
Saydam, A.Z., Taylan, M., 2018. Evaluation of wind loads on ships by CFD analysis. Ocean. Eng. 158, 54–63.
Shearer, K.D.A., T.C., D.R., Lynn, W.M., 1961. Wind tunnel tests on models of merchant ships. Int. Shipbuild. Prog. 8 (78), 62–80.
Shih, T.H., Liou, W.W., Shabbir, A., Zhu, J., 1995. A new k-ε eddy-viscosity model for high Reynolds number turbulent flows – model development and validation. Comput. Fluids 24 (3), 227–238.
Solari, G., Repetto, M.P., Burlando, M., De Gaetano, P., Parodi, M., Pizzo, M., Tizzi, M., 2012. The wind forecast for safety management of port areas. J. Wind Eng. Ind. Aerod. 104–106, 266–277.
Stathopoulos, T., 2002. The numerical wind tunnel for industrial aerodynamics: real or virtual in the new millennium? Wind Struct. 5, 193–208.
Sun, X., Feng, X., Gauri, D.K., 2014. The cruise industry in China: efforts, progress and challenges. Int. J. Hospit. Manag. 42, 71–84.
Thoresen, C.A., Port Designer's Handbook. third ed.. Published by ICE Publishing, One Great George Street, Westminster, London SW1P 3AA, 2014. ISBN 978-0-7277-6004-3.
Tominaga, Y., Mochida, A., Yoshie, R., Kataoka, H., Nozu, T., Yoshikawa, M., Shirasawa, T., 2008. AIJ guidelines for practical applications of CFD to pedestrian wind environment around buildings. J. Wind Eng. Ind. Aerod. 96 (10–11), 1749–1761.
Torre, S., Burlando, M., Repetto, M.P., Ruscelli, D., 2019. Aerodynamic coefficients on moored ships. Proceeding of the 15th International Conference on Wind Engineering, Beijing, China, September, pp. 1–6.
Valčič, M., Prpić-Oršić, J., Vučinić, D., 2020. Chapter: application of pattern recognition method for estimating wind loads on ships and marine objects. Advances in Visualization and Optimization Techniques for Multidisciplinary Research. Lecture Notes in Mechanical Engineering. Springer Nature Switzerland AG, pp. 123–158.
van Berlekom, W.B., 1981. Wind Forces on Modern Ship Forms – Effects on Performance. Swedish Maritime Research Centre.
van Hassel, E., Meersman, H., Van De Voorde, E., Vanelslander, T., 2016. Impact of scale increase of container ships on the generalised chain cost. Marit. Pol. Manag. 43 (2), 192–208.
van Hooff, T., Blocken, B., 2010. Coupled urban wind flow and indoor natural ventilation modelling on a high-resolution grid: a case study for the Amsterdam ArenA stadium. Environ. Model. Software 25, 51–65.
Van Zwijnsvoorde, T., Vantorre, M., 2017. Safe mooring of large container ships at quay walls subject to passing ship effects. International Journal of Maritime Engineering 159, A367–A376.
Versteeg, H.K., Malalasekera, W., 2007. An Introduction to Computational Fluid Dynamics: the Finite Volume Method. Harlow-Longman Scientific & Technical, London.
Wang, W., Wu, T.C., Zhao, D.G., Guo, C.Y., Luo, W.Z., Pang, Y.J., 2019. Experimental-numerical analysis of added resistance to container ships under presence of wind-wave loads. PloS One 14 (8), e0221453 article number.
Wieringa, J., 1992. Updating the Davenport roughness classification. J. Wind Eng. Ind. Aerod. 41–44, 357–368.